Dissertation Type: research

DEPARTMENT OF ENGINEERING MATHEMATICS

Spatio Temporal Dynamics of Human-Mosquito Interaction

Rida Rambli

A dissertation submitted to the University of Bristol in accordance with the requirements of the degree of Master of Engineering in the Faculty of Engineering.

Wednesday 5th August, 2020

Abstract

The main purpose of this research is to see if there is evidence of spatio-temporal patterning, and whether this can be explained by the presence of a Turing instability since this onset generates heterogeneous spatial patterns via a reaction diffusion mechanism. The data observations in this study mostly focus on the emergence of malaria in Uganda which was due to the varied temperature each year, with years 2010 and 2016 having experienced the optimum temperature for mosquito reproduction. However, this alone does not entirely explain the emergence of hotspots in the country. The fundamental of this study is mainly based on Alan Turing's diffusion-driven instability concept. This study investigates the existence of Turing instability in the current spatio-temporal population of the simple Ross and MacDonald(RM) system of mosquitoes and humans. Despite modifying the system by adding superinfection to the recovery term, it was found that the system does not possess any Turing Instability but produced a homogeneous spatial pattern. Finally, we have introduced a new human-mosquito model, based on the knowledge of their dynamics. Turing instability arises in this model, depending on the diffusion rates chosen. In this case, our result displayed heterogeneous spatial patterning and does not settle down in time.

Acknowledgements

I would like to express the deepest appreciation to my supervisor, Professor Alan Champneys for his valued advice and continued support throughout this dissertation. I would also like to thank my personal tutor, Dr Luca Giuggioli for his consistent support throughout my Masters course. Next, I would like to thank David Alonso for providing me early access to his paper and explaining his research through Skype during the early days of my dissertation. Finally, a big appreciation to my parents for giving me daily motivation and emotional support.

Declaration

This dissertation is submitted to the University of Bristol in accordance with the requirements of the degree of MEng in the Faculty of Engineering. It has not been submitted for any other degree or diploma of any examining body. Except where specifically acknowledged, it is all the work of the Author.

Rida Rambli, Wednesday 5th August, 2020

Contents

Chapter 1

Introduction

Mosquitoes, despite being small, can be deadly. They are an impressive means of medium for vector-borne pathogens, posing a risk to more than half of the world's population [9]. This problem has had a detrimental effect on global health, whilst also threatening many economies. The most commonly affected areas are in the tropics and sub-tropical regions. Nevertheless, the pathogen's geographic dispersion is changing because of several factors such as vector control, urbanisation, climate change, human mobility and economic development [11]. This research will mainly focus of the development and analysis of malaria, one of the diseases related to mosquitoes.

Mosquito-borne diseases include malaria, dengue, West Nile virus, chikungunya, yellow fever and Zika fever. These diseases vary in the types of mosquitoes that transmit them to humans. Malaria is transmitted to humans by the *Aenopheles* mosquito, caused by a parasite called *Plasmodium*. Children with severe malaria often develop the following symptoms: severe anaemia, respiratory distress or cerebral malaria. In adults, they frequently experience multi-organ failure. Malaria can lead to death if not treated within 24 hours [23].

1.1 Life Cycle of Malaria Parasites

It is essential to fully understand how malaria develops in order to fully appreciate and understand the importance of this research and also to perceive the history regarding this disease. Malaria occurs due to infection with five species of *Plasmodium* parasite, of which their life cycles are very similar as shown in Figure 1.1.

The first stage is the infective phase whereby infection starts when parasites are injected by a mosquito, and they then travel around the body until the parasites invade liver cells. Here, the second phase takes place, undergoing asexual multiplication stage, allowing the production of multiplied parasites. The blood will then be flooded with more parasites where the second phase of parasite multiplication is initiated, invading new red blood cells. This process is indefinitely repetitive and hence, responsible for the disease, malaria. When the mosquito bites a new host, the cycle begins again [12].

1.2 History of Malaria

Malaria is an ancient disease which was believed been mentioned in Chinese document (∼2700 BC), Egyption papyri(∼ 1570 BC), Mesopotamia clay tablets (∼2000 BC) and as far back as

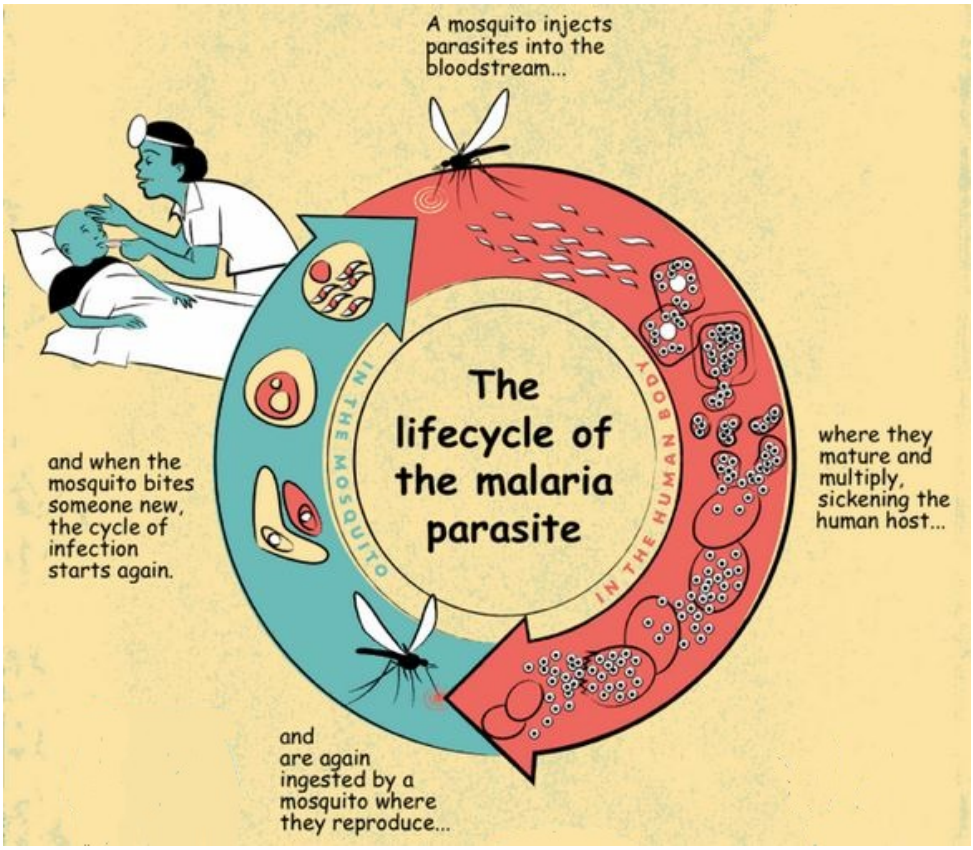

Figure 1.1: Malaria parasite (*Plasmodium*) schematic life cycle taken from [24].

the sixth century BC in the Hindu texts. These historical records were regarded with caution. However, in later centuries, researchers are starting to step onto a firmer base [6].

The early Greeks, such as Homer (850 BC), Hippocrates(400 BC) and Empedocles of Agrigentum (550 BC) were all well aware of the malarial fevers which occurred within people living in swamp areas. The idea that malaria fevers caused by miasmas (bad air) rising from swamps has persisted for over 2500 years. It is widely recognised that the word malaria comes from the Italian word "mal'aria" which brings the meaning spoiled air, although this has been disproved.

The search of malaria intensified with the discovery of bacteria by Antoni van Leeuwenhoek (1676) and the involvement of microorganisms as the source of infectious diseases. The evolution of the germ theory of infection by Louis Pasteur and Robert Koch in 1878-1879 also contributed to malaria research. After the discovery of parasites by Charles Louis Alphonse Laveran in 1880 and the incrimination of mosquitoes as vectors (from 1897 by Ronald Ross), only then the doors to scientific studies became possible [13].

Malaria parasites and the human race have had a long history of evolutionary host-parasite association. The malaria parasite population in Africa has been steadily increasing over the last 10 000 years, whilst also spreading into other continents. This coincides with the growth of the human population and migration due to the dawn of agriculture [35]. The spread of malaria to non-African continents is believed to have been caused by a small population migrating during the Ice Age.

Figure 1.2 shows the plausible maximum global area in which malaria is present, and how this has evolved over time. This map represents all-malaria risk which refers to one or more of the four species of *Plasmodium* causing malaria in human beings.

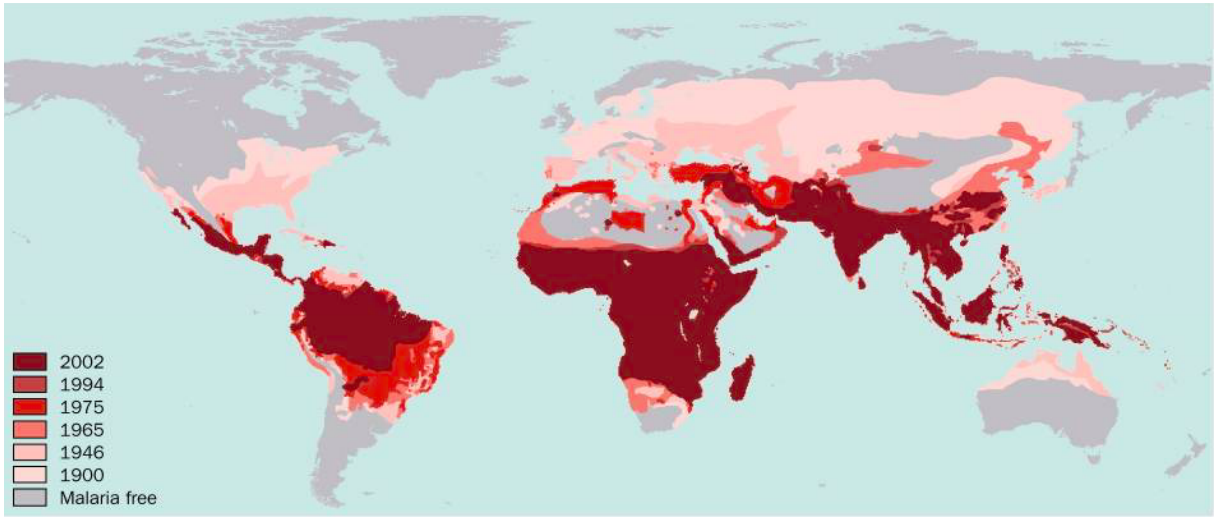

Figure 1.2: Map showing the shrinking spatial extent of malaria from preintervention years until 2002. Figure taken from [11].

The twentieth century saw an unprecedented advance in the success of human control of malaria with a 25.92% decrease of malarious land. Preintervention implementations and vector control efforts have reduced the area of human malaria risk by approximately half, from 53% down to 27% of the Earth's land surface. This information can be seen in Figure 1.3.

Time	Global population	Land area malarious		Countries at risk	Population exposed	
Years	*n*	*km*^{2}	%	*n*	*n*	%
1900	1 158 409 472	77 594 480	53·16	140	892 373 056	77·03
1946	2 391 400 960	58 565 752	40·12	130	1 635 815 808	68·40
1965	3 363 417 344	53 492 988	36·65	103	1 924 360 320	57·21
1975	4 085 759 488	48 075 780	32·93	91	2 121 086 592	51·91
1992	5 419 255 808	43 650 812	29·90	88	2 565 702 144	47·34
1994	5 582 432 256	39 537 020	27·08	87	2 570 555 136	46·05
2002	6 204 095 488	39 758 172	27·24	88	2 996 419 584	48·30
2010	6 807 085 056	39 758 172	27·24	88	3 410 862 080	50·11

Figure 1.3: Table shows global population at risk from malaria (since preintervention(∼1900) to 2010) taken from [11]. The map area distribution was generated using the area at risk of all-cause malaria through time.

The eradication of malaria faces many difficulties including anti-malarial drug resistance, insecticide resistance and the presence of disease carrier with no symptoms, which can be described as asymptomatic. The most effective tools for malaria elimination have been indoor residual spraying and long-lasting insecticidal nets (LLINs). However, more than 30 countries reported resistance to LLINs, with the potential to spread to other areas [20].

Mathematical models strive to play a crucial part in the scientific comprehension of vector-borne disease dynamics. This include informing decisions regarding control and elimination, with the ability to sum up complex spatio-temporal dynamics. Despite increasing interest in the

implications of spatial process for vector-borne disease dynamics, the assumption of spatially homogeneous transmission was only accounted for.

The Kermack-McKendrick model, known as the SIR model, has been used to study epidemic cases. The model is divided into three cases which are susceptibles (S), infected (I) and recovered (R) individuals [2].

$$\frac{dS}{dt} = -\beta IS, \tag{1.1}$$
$$\frac{dI}{dt} = \beta IS - \gamma I, \tag{1.2}$$
$$\frac{dR}{dt} = \gamma I. \tag{1.3}$$

When the infected (I) and susceptibles (S) are in contact, they result in new infections. The rate at which this new infection takes place in this simple model is βSI for some constant $\beta > 0$. When this infection occurs, the infected individuals will enter the infected class from the susceptible class, so we have have the first differential equation (Eq 1.1).

The next case that can occur is that infected individuals will recover, at the rate γI for some constant $\gamma > 0$. Thus, we have the last two differential equations (Eq 1.2 and 1.3). The total population is constant because the differential equations sum up to zero.

An example of a malaria model is the Ross-Lotka model (Eq 1.4) [30]. The model focuses more on the mathematical details instead of the entomological aspects. Ross considered births and deaths in both humans and mosquitoes to be equal respectively so the populations would be in their steady state for analysis.

$$\begin{aligned} \frac{dY}{dt} &= maz(H - Y) - rY, \\ \frac{dX}{dt} &= aI_{HM}x(M - X) - d_M X, \end{aligned} \tag{1.4}$$

where H is the human population density, Y is the number of infectious humans and X is the number of infectious mosquitoes. The other parameters are daily rate each human recovers from infection (r), mosquito instantaneous death rate (d_M), probability a mosquito becomes infected after biting an infected human (I_{HM}), malaria rate (x), ratio of mosquitoes to humans (m), the proportion of mosquitoes that feed on humans each day (a) and the fraction of infectious mosquitoes (z).

Most studies of vector-borne diseases do not take specific account of spatial effects such as in ([31],[10],[32]). As yet, the rule of nature incorporates heterogeneous transmission [7], whereby spatially heterogeneous transmission would arise as a result of spatial variation in vector habitat, control, temperature and rainfall. These factors influence vector reproduction, survival and vector-host encounters.

Pathogen transmission dynamics are linked with the hosts movement among patches with various transmission rates. Some patches may have environmental conditions that promote disease spread and hotspots. However, without immigration of infectious hosts from hotspots, some patches may not be able to sustain the disease in the area [5]. For most aspects, control strategies commonly focus on decreasing the ability of mosquitoes to carry the disease with some successes and some failures such as malaria elimination form Puerto Rico [18] and malaria control efforts in Burkina Faso [4] respectively.

1.3 Stakeholder Relevance

This study would be beneficial for Centers for Disease Control and Prevention (CDC) sectors to understand the emergence of heterogeneous malaria patchiness. Hence, allowing a robust malaria control effort as parameters can be manipulated to fit a country's data on this disease.

The next stakeholder would be World Health Organization (WHO) to record changes in malaria spatial pattern over time. Since their work and report are recognised world wide, it would be a platform to increase awareness on malaria research and advancement.

1.4 Outline

Now that we have a brief overview of the development of malaria parasite and its history, we will next look into the recent cases of this disease and the dynamic of human and mosquito populations. We have outlined a plausible hypotheses that might cause malaria patchiness emergence which include temperature variation, bistability and Turing instability.

In the next chapter, we will analyse the spatial distribution of affected children (age 2-10) across the world through data visualisation and temperature variation. Then, we will focus on recent malaria outbreak in Uganda and the relationship between these cases and the varying temperatures within 4 years (2010, 2012, 2014 and 2016).

Chapter 3 will look into the mathematical background of the Ross-MacDonald (RM) model and the derivation of the system of equations. This section also explains Turing instability in detail.

Chapter 4 will be an analysis of an extended RM model, which includes existence of bistability in the system. We will also investigate if there is any Turing instability of this system and observe the evolution of spatial pattern based on our reaction-diffusion computation.

Chapter 5 is an analysis of the extended human-mosquito interaction model which we have newly introduced. The same method will be implemented from the latter chapter to this section. We will investigate the correlation between Turing instability and the existence of spatial patterns.

The final chapter concludes the results drawn from our research, together with critical evaluations and discussions for future works.

Chapter 2

Data Observations and Analysis

2.1 Global Malaria Outbreak

Malaria still remains a global health concern and a main cause of mortality worldwide. A continued effort in global control has resulted in the disease morbidity to be reduced from 13% to 9% between years 2005 to 2015 based on [33].

The understanding of spatial and temporal dynamics of malaria is important for sustainable control and elimination interventions [15]. Spatio-temporal analysis of malaria [17] predicted annual risk of malaria for children aged between 2 to 10 years. This was implemented using the geostatistical model fitted on a limited number of parameters which were age, location, time of survey and sample of numbers. Spatio temporal analysis studied were [3]:

1. **Rainfall and malaria**: More malaria cases in raining season due to high number of breeding grounds. The study showed a definite relation with rainfall.
2. **Temperature and malaria**: Both positive and negative correlation with temperature were shown in this study with optimum temperature between 20-35° C.
3. **Vegetation and malaria**: Again, both positive and negative correlation with malaria diseases were recorded. Vegetation is a suitable breeding sites, developing in more malaria occurrence and transmission.
4. **Other factors and malaria**: Population density and water bodies showed different results. There were fewer malaria cases in areas with high population and vice versa. Likewise, different types of water bodies such as rivers, streams and ponds showed a disparity in malaria incidence.

Since 2000, the increased effort of malaria control interventions has reduced global mortality and morbidity caused by the disease (refer Figure 2.1). However, declines have not been universal, with alarming levels of malaria still existing in many countries. Given the rise in the availability if geospatially resolved data, (e.g. Malaria Atlas Project (MAP)), the malaria control programmes have adopted high-resolution maps to characterise spatially heterogeneous patterns of malaria risk and accordingly target areas of high burden more efficiently.

In [34], the *Plasmodium falciparum* parasite rate and clinical incidence models for sub-Saharan Africa were updated and refined. With the availability of open source malaria data which can be found in Malaria Atlas Project, Figure 2.1-2.3 were obtained. Between years 2002-2005, there was a peak in global *Plasmodium falciparum* incidence in all regions as shown in Figure 2.1. However, it can be seen it is mainly dominated by Sub-Saharan Africa.

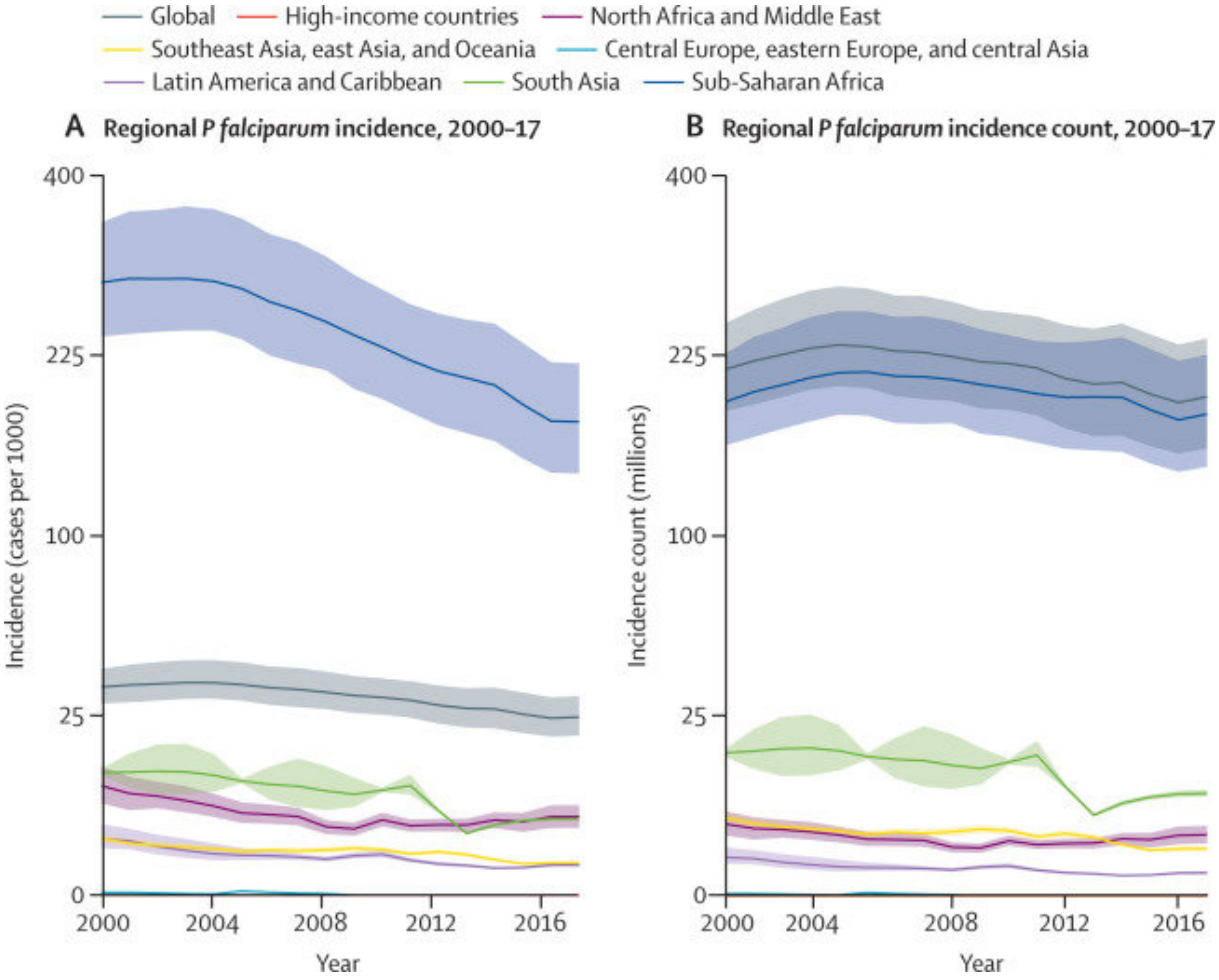

Figure 2.1: Diagram above shows the regional distribution of *Plasmodium falciparum* (A) incidence(cases per 1000) and (B) incidence count(in millions) taken from [34]. The corresponding colour bands behind the mean lines represent the 95% uncertainty intervals. The total population in all endemic countries within each region were used to calculate the rates.

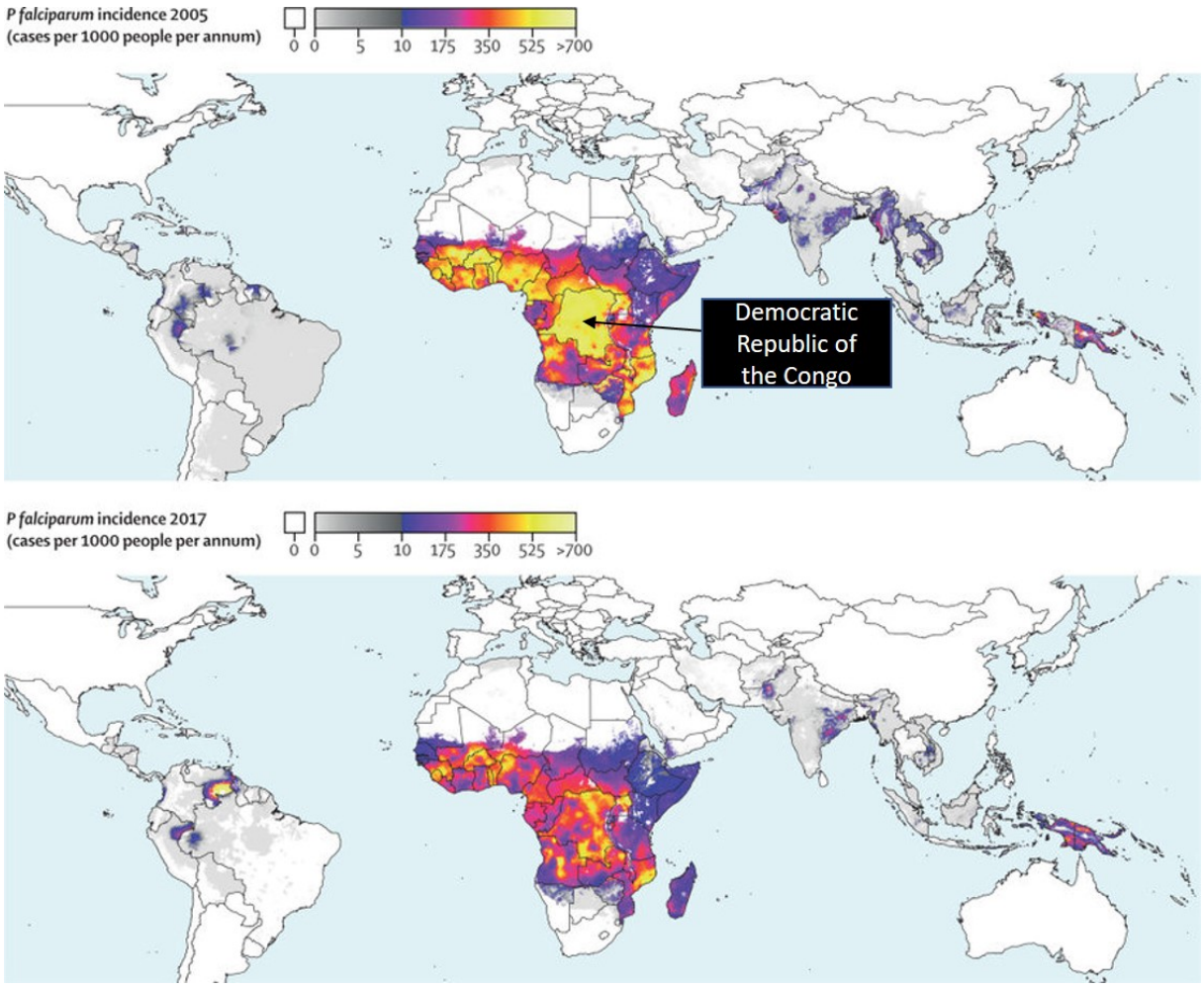

Figure 2.2: Diagram shows the spatial distribution of all-age affected by *Plasmodium falciparum* incidence in 2005 and 2017 which are in top and bottom respectively taken from [22].

The global maps for *Plasmodium falciparum* affecting victims of all-age can be seen in Figure 2.2, which represented outbreaks in 2005 and 2017 respectively. The colour scaling is split for a better distinction within low endemic areas. There is a linear scale between rates of 0 and 10 (displayed by grey shades) and a second linear scale between 10 and 1000 with a range from purple to yellow. Regions not affected with *Plasmodium falciparum* endemicity are shown in white. These maps illustrate the improvement that has been implemented in reducing the burden of *Plasmodium falciparum* and the areas of continuing concern. Democratic Republic of Congo had a serious case of malaria in 2005 as almost the entire country experienced high malaria incidence. However, the map shows an overall improvement in the country in 2017.

Malaria affects children more severely than adults. Hence, there are more clinically recorded cases among children than any other ages. There are three principal ways in which malaria contributes to mortality in young children. First is a serious acute infection which often presents as coma (known as cerebral malaria) and seizures. This may kill an infected child quickly and directly. Second, recurring malaria infections contribute to the progress of severe anaemia which increases the risk of mortality. The third is low birth weight which is the affect of malaria infection in pregnant woman. Moreover, recurrence of malaria infections make young children susceptible to other common childhood illnesses thus indirectly contributing to mortality [29]. Hence, our next focus would be to study and observe the spatial distribution of the *Plasmodium falciparum* parasite rate for children aged 2-10 years old.

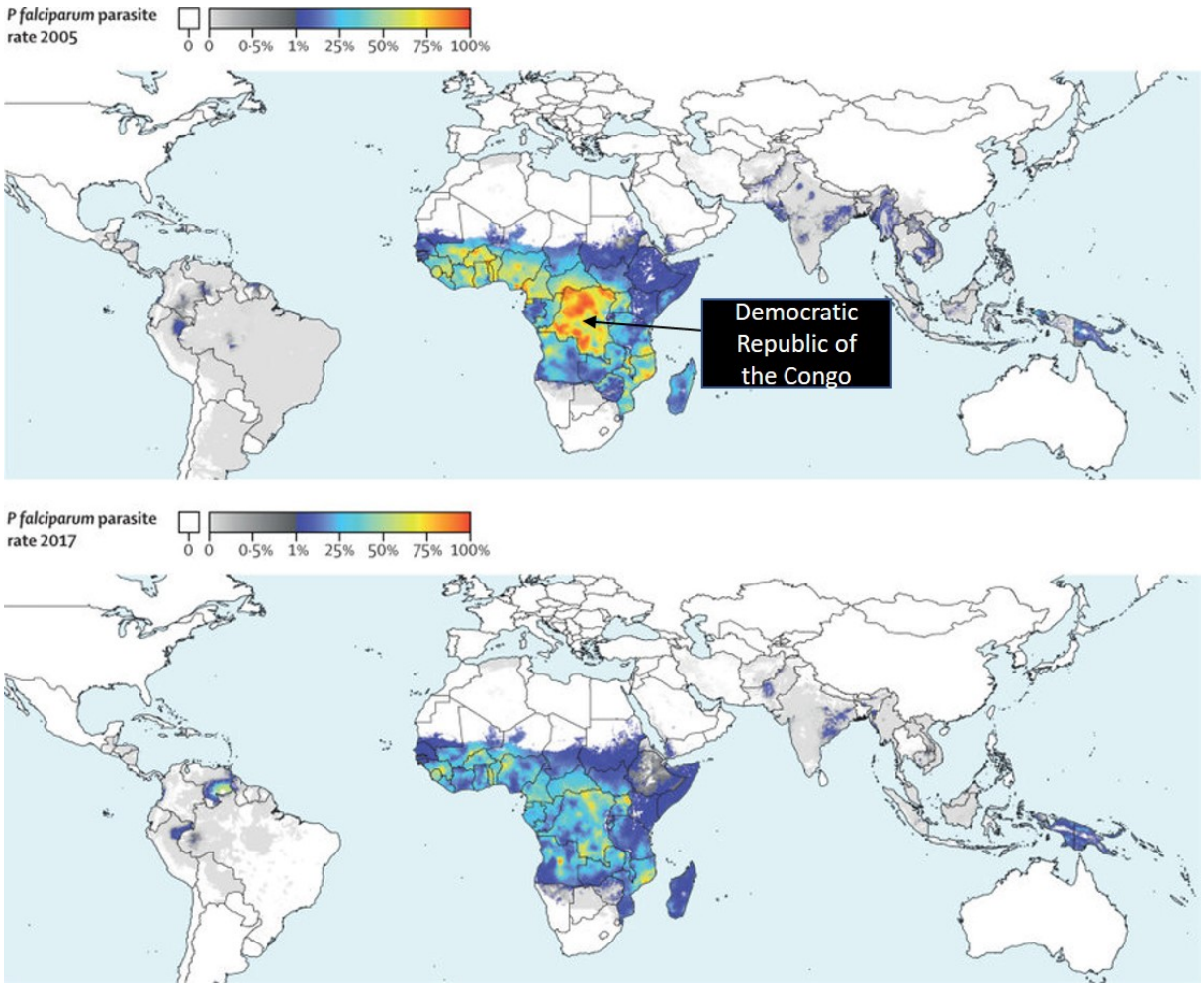

Figure 2.3: Diagram shows the spatial distribution of P falciparum parasite rate for children aged 2-10 years of age in 2005 and 2017 shown in top and bottom maps respectively.

The index for malaria transmission intensity is commonly known as the *Plasmodium falciparum* parasite rate (PFPr). Figure 2.3 shows the spatial distribution of age-standardised(2-10 years of age) *Plasmodium falciparum* parasite rate(PFPr) in 2005 and 2017. Again, note that the colour scaling is to differentiate within the low endemic areas with one linear scale between 0 to 10% shown in grey shades and a second linear scale between 10% and 100% shown from blue to red. The regions without any malaria endemic are displayed in white. As can be seen from the diagram, there has also been an overall improvement in Democratic Republic of the Congo in 2017 compared to 2005. There are no orange patches which represent 75%-100% *Plasmodium falciparum* parasite rate in children aged 2-10 years old. However, with yellow patches (75%*Plasmodium falciparum* parasite rate) still existing in Democratic Republic of the Congo, it is in our interest to see if this affects the neighbouring country, Uganda.

2.2 Case : Uganda

It has been proven as stated in [19], that the optimal temperature for malaria transmission is dramatically lower than previously predicted. The predicted optimal transmission has been 31°C. This record was based on field observations of outbreak dating back almost a century. With a realistic ecological assumptions about mosquitoes thermal physiology and nonlinear thermal

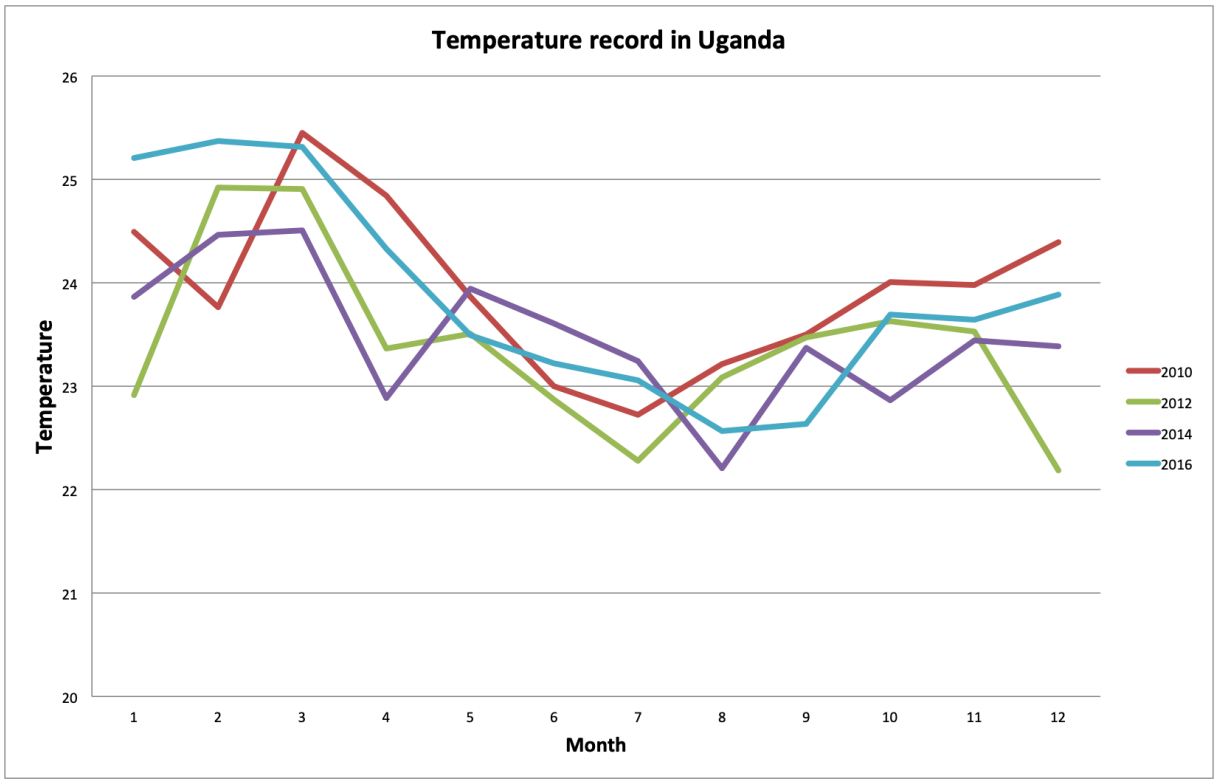

Figure 2.4: Diagram shows the temperature record in Uganda obtained from [26].

responses, the optimal malaria transmission was found to be at 25°C and with temperature above 28°C, the transmission will diminish.

Figure 2.4 shows the temperature in Uganda, which was obtained from Climate Change Knowledge Portal open source data [26]. As can be seen in the diagram, there is no overall drastic changes in temperature. However, the temperature is well within our range in March in 2010 and January till March in 2016 which is just above 25°. Intuitively, we will expect there were higher malaria outbreak in 2010 and 2016.

As shown in Figure 2.5, the malaria transmission intensity for children 2-10 year olds is affected by temperature variable. The parasite rate was the highest in 2010 and gradually decrease over the years, with the lowest rate seen in 2014. In 2015, the parasite rate started to increase gradually and in 2016 there was a significant increase. In conclusion, this parasite rate is proportional to the temperature in the the dry season, occurring from January till March. Wet season occurs from March till May which provide optimal breeding ground for this insects. Hence, with the combination of temperature variation and occurring seasons, explains the increase in malaria in 2010 and 2016.

Based on Figure 2.6, the maps show travelling hot spots of high malaria parasite rate which are indicated in orange-yellow patchiness (indicates >50% parasite rate). In 2012, only one hotspot from 2010 remained which is in the South East. However, in 2016, there is an emergence of a larger hotspot in the North. The initial assumption would be that the hotspots were affected by the geographical areas of the country itself.

As shown in Uganda map, areas in Murchison National Park, Pian Upe Game Reserve and Mount Elgon National Park were never affected, hence the white spots. These areas are protected, with less human population. Thus, no malaria was detected in these regions. The patchiness occurred at low areas and outside the nature reserves where there are higher number of people. The South Western (compromised of tropical rainforests) districts and Central regions have a much

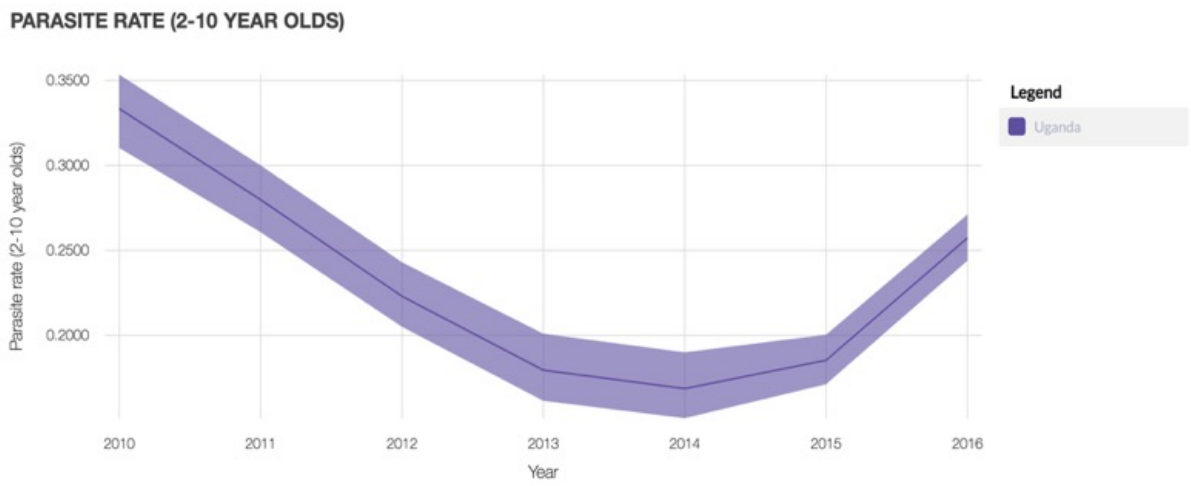

Figure 2.5: Plot shows the predicted parasite rate for children 2-10 year olds by their respective year. The corresponding coloured bands behind the mean lines represent the 95% uncertainty intervals. Data was collected from [22].

lower parasite rate. This result shows geographical area plays a role in malaria transmission intensity.

2.3 General Observations

Hence, our findings have shown that the overall malaria dynamic is affected by temperature variation with the optimum temperature between 25°C-28°C. Higher ground regions are not affected by malaria, as there are less human density and have low temperature. Although these factors affect malaria intensity, they do not show any evidence to spatial pattern correlation yet. Hence, we will next investigate our second plausible hypotheses which includes bistability to see if this affect spatial pattern.

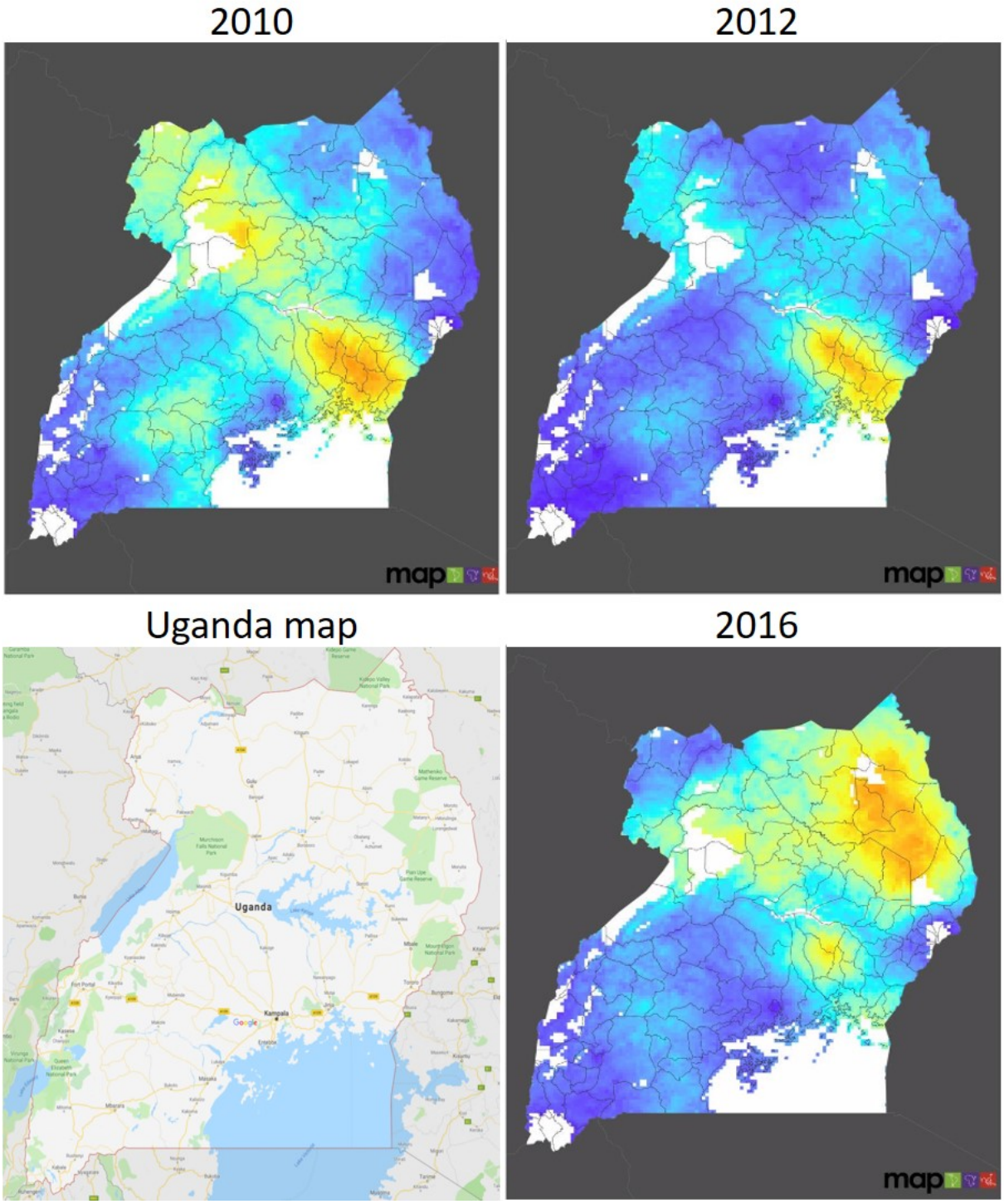

Figure 2.6: Map showing parasite rate rate for Plasmodium falciparum malaria for children two to ten years of age taken from [22] and Uganda map obtained from Google Maps. There is emergence of hot spots based on this maps. The intensity of parasite rate is represented in (a)orange(75%-100%), (b)yellow(60%-75%), (c)light blue(25%-60%), (d)dark blue(1%-25%) and white (%0).

Chapter 3

Mathematical Background

3.1 Basic Ross-MacDonald(RM) Model

The modelling of vector-borne infections fundamentally began with the papers by Ross on malaria, "*The Prevention of Malaria*" [27]. There are three areas of biological importance from his study which are (1) basic research, (2) malaria transmission and epidemiology and (3)the identification in the parasite life-cycle for a more effective intervention. The last area was immediately identified and recognised, deriving in the ratification of environmental vector control effort. These were adopted in the 1930s with the introduction of effective insecticides together with the new antimalarial drug, forming the foundation of the successful global control campaign during the 1950s and 1960s [14].

Ross assumed that the malaria dynamics could be simplified by two equations that describe the prevalence of malaria disease in both the human and mosquito hosts. This formation has created the basic core of models for malaria, and also most other vector-borne diseases for the past century. These models incorporated further information relating to the cause of the disease development, to build a better approximation.

This section portrays the full model represented by a system of Ordinary Differential Equations (ODE's) which are purely temporal. Malaria transmission within the human and mosquito populations is defined by two coupled submodels respectively. The formulation below builds upon the Ross and MacDonald classical model. Note that the values and meanings of the parameters in submodels can be obtained in Table(A.1) in the Appendix section.

Human Population Model

Using the method from [1], we will start by creating submodels which subdivide the human population into different classes. There are two classes for infected humans which are represented by those who receive clinical treatment (C) and those who do not receive clinical treatment (I). As soon as individuals naturally recover from malaria, they will enter a refractory period (a short period of time in which infection cannot be generated) and are immune to the disease. Until they return to the susceptible class (S), this group of individuals can not be re-infected by malaria. Thus, the immune class does not contribute to the transmission. In order to implement superinfection, the infectious period is dependant on the infectious bites exposure by the mosquito (this defines the intensity of transmission). The ODE systems for the human population model are written as

$$\frac{dS}{dt} = B - \beta S + \sigma R - \delta_H S + \rho C, \tag{3.1}$$
$$\frac{dE}{dt} = \beta S - \delta_H E - \gamma_H E, \tag{3.2}$$
$$\frac{dI}{dt} = (1-\chi)\gamma_H E - \eta\beta I + \nu C - rI - \delta_H I, \tag{3.3}$$
$$\frac{dR}{dt} = -\sigma R + rI - \delta_H R, \tag{3.4}$$
$$\frac{dC}{dt} = \chi\gamma_H E + \eta\beta I - \nu C - \rho C - \delta_H C. \tag{3.5}$$

In this system, the average time of exposed class is $\frac{1}{\gamma_H}$ and is exponentially distributed. The restoration of susceptible through births (B) and mortality (δ_H is per capita human mortality rate) are regarded to balance each other . This is to ensure that the total human population (N) remain constant. The susceptible group becomes infected at a per capita rate of β which is the force of infection. Fundamentally, $\frac{1}{\beta}$ can be calculated approximately from the mean age at which children first acquire malaria with the assumption there is constant mosquito exposure. However, only a fraction of infections, represented by χ, are detected and clinically treated. The term (1-χ) represents undetected infections. The non-clinically treated (I) can still regain infection and be detected upon reinfection but the per capita rate of force of infection , β is decreased by a factor of η. The rates of clearance for clinically treated (C) and non-clinically treated (I) are given by ρ and r respectively.

Mosquito Population Model

Now, let us consider the mosquito life cycle which consists of four different stages : egg, larva, pupa and adults. Within 24 hours mosquito larvae develop from eggs. The larval stage is aquatic and lasts about couple of weeks. The pupal stage is around 1 to 4 days. The development period is dependent on the mosquito species and the surrounding temperature. The adult stage is longer and predicted by decaying exponential. From an epidemiological view, the larval (L) and adult phases (M) are the most crucial. Thus, mosquito dynamics population can be obtained by just considering the two stages in the mosquito life cycle which are shown below [1]

$$\frac{dL}{dt} = aN_L M(\frac{K_0 - L}{K_0}) - \delta_L L - d_L L), \tag{3.6}$$
$$\frac{dM}{dt} = d_L L - \delta_M M. \tag{3.7}$$

The number of individuals recruited into the larval state per adult female mosquito is determined by the per capita rate of reproduction. Since females need to feed on blood to produce eggs, the reproduction depends heavily on the biting rate, a. d_L represents the per capita rate of the emergence of adult mosquitoes from the larvae phase. The larval growth is controlled by the carrying capacity K_0 in a straightforward logistical way which strongly corresponds to water availability. In general, K_0 fluctuates seasonally with rainfall. The values and meanings for the parameters are shown in Table A.1.

Hence, this particular model can readily be coupled with the disease dynamic corresponding to the human population model. Commonly, there are three parts to the adult mosquito population : susceptible non-infected mosquitoes (X), infected non-infectious mosquitoes (V) and infectious

mosquitoes (W). Let y be the fraction of the human population transmitting the parasite to the mosquito, then

$$\frac{dX}{dt} = -cayX - \delta_M X + d_L L, \tag{3.8}$$
$$\frac{dV}{dt} = cayX - F(t) - \delta_M V, \tag{3.9}$$
$$\frac{dW}{dt} = F(t) - \delta_M W. \tag{3.10}$$

The rate at which infected mosquitoes (V) turn into infectious mosquitoes(W) is denoted as $F(t)$. Here, we take into consideration the time taken for a *Plasmodium* parasite to mature and reach infecting stage within the mosquito vector body (sporogonic phase).

Adding Eqs 3.8-3.10 sums up to Eq 3.7. We consider that the total mosquito dynamics is not affected by malaria transmission since there is no factual proof on a detrimental effect of *Plasmodium* infection on adult female mosquitoes.

Hence, based on the full model obtained from the human submodels obtained from Eqs 3.1-3.5 and the mosquito submodels of Eqs 3.6-3.10, they can be simplified into the original Ross and MacDonald (RM) formulation

$$\frac{dw}{dt} = cay(m - w) - \delta_M w, \tag{3.11}$$
$$\frac{dy}{dt} = baw(1 - y) - \delta_H y, \tag{3.12}$$

where number of infectious mosquitoes and infectious human individuals are both per total human population, denoted as w and y respectively. All the parameter values can be obtained from Table A.2. The following assumptions were implemented and required :

1. human and mosquito populations are constant,
2. no consideration of external force infection,
3. no immunity,
4. mosquito exposure does not affect recovery rates,
5. a single infectious human class consists of detected and non-detected human infections,
6. mosquitoes and humans instantly become infectious following an infectious bite and
7. absence of E,R and C classes.

Thus, with these assumptions, the human submodel is simplified to Eq 3.12 when the human population size, N remains constant.

3.2 Turing Instability

This section explains Turing Mechanisms which would be implemented later to analyse Ross's models. In 1952, Alan Turing proposed that under certain conditions, there exist a reaction and diffusion in chemicals which would create steady state heterogeneous spatial patterns [21]. The governing equation for the reaction diffusion mechanism is

$$\frac{\partial \mathbf{c}}{\partial t} = \mathbf{f}(\mathbf{c}) + D\nabla^2\mathbf{c}, \tag{3.13}$$

where $\mathbf{c}$ represents morphogen concentrations, $\mathbf{f}$ represents reaction kinetics and D represents the diagonal matrix of positive constant diffusion reactions. Say we have two models of chemical species (which later on will be introduced as human and mosquito population), $A(\mathbf{r}, t)$ and $B(\mathbf{r}, t)$. The system of equation is then expressed as

$$\begin{aligned} \frac{\partial A}{\delta t} &= F(A, B) + D_A\nabla^2 A, \\ \frac{\partial B}{\delta t} &= G(A, B) + D_B\nabla^2 B, \end{aligned} \tag{3.14}$$

where F and G are both the kinetics and will always be non-linear.

Turing's concept is simple yet a profound one. He found out that if in the absence of diffusion (i.e when D_A=D_B=0), A and B turn to a linearly stable uniform steady state. Hence, under certain conditions which shall be derived, spatially inhomogeneous patterns can develop by diffusion driven instability when $D_A \neq D_B$. This was acknowledged as novel concept as the diffusion term is often considered as a stabilising process. Based on the following informative, yet unrealistic analogy, we can see instinctively how diffusion can be destabilising.

Presume that there is a large amount of villagers concentrated in one area of the village. Let us represent mosquitoes as activators and villagers as inhibitors. Female mosquitoes will be attracted to the area as they can feed on villagers in order to produce eggs. Mosquitoes carry parasites in them, hence why we label them as activators as they spread diseases. Villagers affected by the disease will then travel to the hospital to get treatment and in return stop the spreading of mosquito disease (as there will be less food for the mosquitoes). Without the presence of these villagers, mosquitoes will be less attracted to the area, hence the villagers are indeed inhibitors in this case.

The setting for spatial pattern is then as bellow:

1. The mosquitoes, which are the activator reactants start to spread in the village, have a diffusion coefficient of D_M. When the villagers hear the news about the malaria endemic in the village, they would move away from the area. The villagers have the diffusion coefficient of D_V, whereby $D_M > D_V$.
2. But if the mosquitoes catch up on the villagers, more control efforts will be incorporated to kill them or repel these mosquitoes.
3. Hence, there will be an area where there will be more dead mosquitoes, confined to a finite domain which is dependent on the diffusion coefficients of the reactants.
4. Now, let us consider the patchiness of mosquitoes (known as hotspots) in the village. Thus, the process would result in final spatial heterogeneous steady state distribution as there will be fewer mosquitoes in some areas, whilst higher in other areas of the village. Together with a spatial distribution of villagers at each hotspot, the above scenario (1-3) would take place.
5. If both the mosquitoes and villagers diffuse at the same rate, no such spatial pattern could take place.

A reaction diffusion system displays diffusion-driven instability, known as Turing instability. This occurs when at small perturbations without diffusion, the homogeneous steady state is

stable. However, when the diffusion is present, the homogeneous steady state will be unstable to small spatial perturbations. The theory of instability in biology is generally applied to the context of ecology. In other words, a uniform steady state turns unstable to small perturbations and there will be some temporal oscillatory behaviour within the populations.

Nevertheless, instability in our context refers to a different meaning. The main method affecting the spatially inhomogeneous instability is diffusion. Diffusion decides the evolution of spatial patterns [21]. The selection of pattern (or mode) is a crucial aspect of the analysis which will be shown later in this chapter. Reaction diffusion systems can be scaled and non-dimensionalised to the general form (Eq 3.15), given the zero flux boundary conditions and initial conditions

$$\begin{aligned} u_t = f(u,v) + D_1\nabla u, \qquad v_t = g(u,v) + D_2\nabla v, \\ (\mathbf{n}\cdot\nabla)\begin{pmatrix} u, \\ v \end{pmatrix} = 0, \quad \mathbf{r} \quad on \quad \partial B; \quad u(\mathbf{r},0), \quad v(\mathbf{r},0) \quad \text{given}, \end{aligned} \tag{3.15}$$

where the diffusion coefficients are denoted by D_1, D_2. The reaction kinetics $f(u,v)$ and $g(u,v)$ and diffusion coefficients determine the capability of the systems to generate Turing instability. The closed boundary of the reaction diffusion domain B is denoted by ∂B with n being the unit normal outward to ∂B. The corresponding homogeneous state (u_0, v_0) of Eq 3.15 is the positive solution of

$$f(u,v) = g(u,v) = 0. \tag{3.16}$$

Since we are interested with diffusion-driven instability, we first need to confirm that without spatial dependency, the system is stable. Below is the derivation for the conditions for the latter to hold : Without spatial variance, u and v satisfy

$$u_t = f(u,v), \qquad v_t = g(u,v). \tag{3.17}$$

Linearising about the steady state (Eq 3.16) by setting

$$\mathbf{w} = \begin{pmatrix} u-u_0 \\ v-v_0 \end{pmatrix}, \tag{3.18}$$

and for $|\mathbf{w}|$ small, Eq 3.16 becomes

$$\mathbf{w}_t = A\mathbf{w}, \qquad A = \begin{pmatrix} f_u & f_v \\ g_u & g_v \end{pmatrix}_{u_0,v_0}, \tag{3.19}$$

where A represents the stability matrix and we want to find the solutions in the form

$$\mathbf{w}_t \quad \propto \quad e^{\lambda t}, \tag{3.20}$$

where λ denotes the eigenvalue. If Re $\lambda < 0$, the steady state is $\mathbf{w} = 0$ since the perturbation $\mathbf{w} \to 0$ as $t \to \infty$. Thus, the solutions for the eigenvalues λ can be determined as follow

$$|A - \lambda I| = \begin{vmatrix} f_u - \lambda & f_v \\ g_u & g_v - \lambda \end{vmatrix} = 0, \tag{3.21}$$
$$\lambda^2 - (f_u + g_v)\lambda + (f_u g_v - f_v g_u) = 0.$$

Hence, linear stability(Re λ) is guaranteed if

$$trA = f_u + g_v < 0, \qquad |A| = f_u g_v - f_v g_u > 0. \tag{3.22}$$

This condition in Eq 3.22 implies f_u and g_v to have opposite signs. Now, let us linearise about the steady state for the full reaction diffusion system (Eq 3.15). Thus, we will obtain

$$\mathbf{w}_t = A\mathbf{w} + D\nabla^2\mathbf{w}, \qquad D = \begin{pmatrix} D_1 & 0 \\ 0 & D_2 \end{pmatrix}. \tag{3.23}$$

We need to determine $\mathbf{W}(\mathbf{r})$ being the time-independent solution (r) of the spatial eigenvalue problem defined below in order to solve the system of equations

$$\nabla^2\mathbf{W} + k^2\mathbf{W} = 0, \quad (\mathbf{n}\cdot\nabla)\mathbf{W}, \quad for \quad \mathbf{r} \quad on \quad \partial B, \tag{3.24}$$

where here eigenvalue is represented by k and is known as the wavenumber. Now, let $\mathbf{W}_k\mathbf{r}$ be the eigenfunction corresponding to the wavenumber k and the zero flux boundary condition is satisfied by $\mathbf{W}_k\mathbf{r}$. We look for solutions $(\mathbf{w}(\mathbf{r}, \mathrm{t}))$ of Eq 3.23 in the form

$$\mathbf{w}(\mathbf{r}, \mathrm{t}) = \sum_k c_k e^{\lambda t}\mathbf{W}_k\mathbf{r}, \tag{3.25}$$

where a Fourier expansion of the initial conditions in terms of $\mathbf{W}_k\mathbf{r}$ determines the constants, c_k and temporal growth is determined by λ. By substituting this system into Eq 3.23 and 3.24 and cancelling $(e^{\lambda t})$, we obtain for each k

$$\lambda\mathbf{W}_k = A\mathbf{W}_k + D\nabla^2\mathbf{W}_k, \tag{3.26}$$
$$= A\mathbf{W}_k + Dk^2\mathbf{W}_k. \tag{3.27}$$

The nontrivial solutions for $\mathbf{W}_k$ are required in order for λ to be determined by the characteristic polynomial roots

$$|\lambda I - A + Dk^2| = 0, \tag{3.28}$$

where now the eigenvalues λ are expressed as a function of wavenumber, k. $\lambda(k2)$ is known as the dispersion relation. It instantaneously gives the initial growth rate or pattern decay of different sizes. Dispersion relation is important as it immediately shows whether patterns can grow. The two fundamental characteristics of $\lambda(k)$ are (a) the spatially featureless state(i.e $k = 0$) is stable and (b) there is a small band of wavelengths which can grow. In general, tuning one of the model parameters will allow the dispersion relation to achieve the qualitative shape. The analysis of the $\lambda(k)$ is informative as they instantly show which spatial patterns (i.e eigenfunctions) grow exponentially in time and are linearly unstable [21].

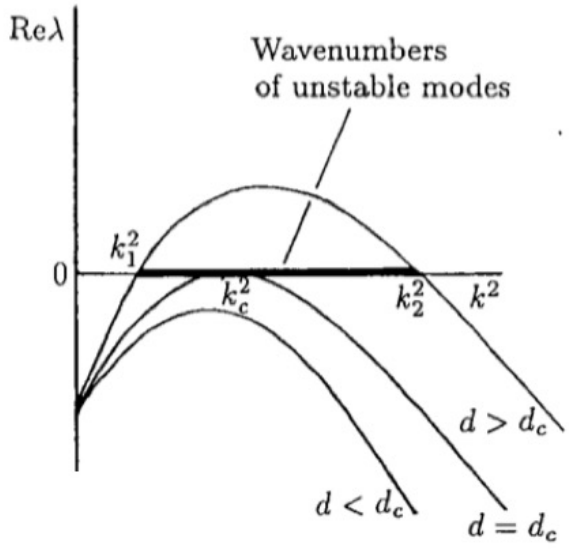

Figure 3.1: Plot of $\lambda(k^2)$ against k^2. d_c is the value for critical d which is denoted as D in Eqn 3.23. When $d > d_c$ there is a range of $k_1^2 < k^2 < k_2^2$ which are linearly unstable. Turing instability arises when there exists $\mathrm{Re}\lambda > 0$.

Hence, based on Eq 3.22, we will obtain two possibilities which are either $f_v < 0$ and $g_u > 0$ or vice versa and they both refer to two different reactions which are illustrated schematically in Figure 3.2. Let us recall that the activator is the reactant that promotes growth and the inhibitor is the opposite. In Figure 3.2(a), the activator is u which also activates itself and v is the inhibitor and also inhibits itself (by referring to the signs of f_u and g_v).

The inhibitor must diffuse faster than the activator for formation pattern to occur. In Figure 3.2(b), it shows that v inhibits itself but also an activator to u (because arrow pointing into u is positive) but still diffuses faster.

The difference between these two cases are the direction of pattern development along the unstable manifold. Figure 3.2(a) has two species at high/low density in the same region as shown in Figure 3.2(c) (refer to the one arrow denoting only one direction). However, in Figure 3.2(b, both species grow in the opposite region as in Figure 3.2(d). This denotes if u density is high, then v density is low and vice versa.

Thus, having the understanding of the Jacobian matrix will simplify our problem as it can be observed quickly. The respective phase planes in the vicinity of their steady states for the two cases are shown in Figure 3.2(e) and Figure 3.2(f).

Let us denote u and v as the human and mosquito respectively for Figure 3.2(e). At high mosquito density, the human density decreases. Near the steady state (the intersection), the humans benefit from each other such that when their number increases, they are temporarily amplified. Mosquitoes reduce in number if the mosquito-to-human ratio is high, but grow otherwise.

Now, let us focus on Figure 3.2(f). Here, we represent mosquito as u and human as v. In this case, when both the human and mosquito densities are in the vicinity of the steady state, the rise in the number of mosquitoes is temporarily amplified. This could occur because when there is a high number of mosquitoes, they breed more and feed on more humans. The difference between this case and Figure 3.2(e) is now the humans disperse at a higher rate. Thus, we want to obtain a figure similar to either Figure 3.2(e) or (f) when we solve the RM classical model.

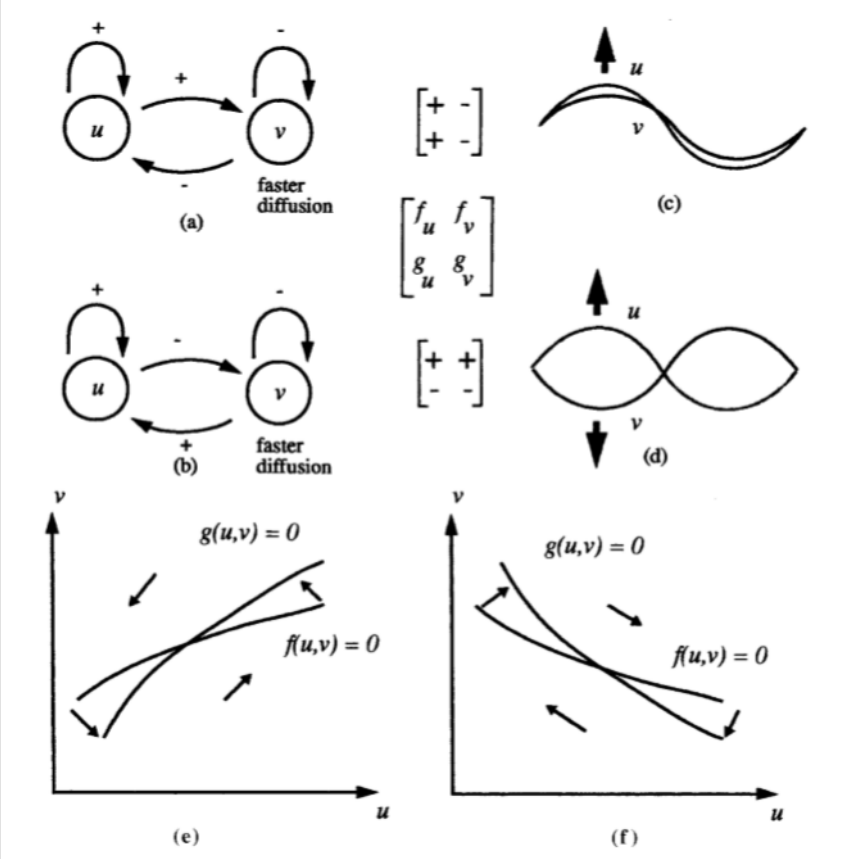

Figure 3.2: Two cases of diffusion-driven stability with different signs of f_v and g_u. (a) u activates both itself and v, whilst v inhibits both. The growing pattern for this case is shown in (c). (b) u activates itself but inhibits v, whilst v inhibits itself but activates u. The resulting pattern is shown in (d). (e) and (f) are the phase planes for the respective cases. Arrows illustrate change of direction affected by reaction without diffusion.[21]

With this fundamental knowledge of Turing instability, we will next analyse the possibility of spatial pattern in classic RM Model and a new human-mosquito model.

Chapter 4

Extended Ross-MacDonald(RM) Model

In this section, there is an introduction of a new term to Ross's original model which is the possibility of superinfection in the human hosts. This concept was introduced by David Alonso and Mercedes Pascual [1] which will be discussed and analysed throughout this chapter.

Superinfection is the reinfection of asymptomatic hosts (hosts that have become infected with a pathogen but display no symptoms) before they are cleared from a former infection [1]. Having this additional detail, it creates the likelihood for break points in the prevalence of infected hosts, which is the abrupt transitions that characterise malaria's reaction to control in different areas.

David Alonso mentioned that ignoring the possibility of superinfection can potentially lead to severe misunderstanding in the analysis of malaria distribution patterns and essentially the design of control efforts for similar vector borne diseases.

4.1 Bistability Analysis

To accentuate the conclusion that superinfection always produces the possibility of bistability, we introduce conditions for model of parameters under which the simple RM model will exhibit this behaviour. The RM model assumes that :

1. both human and mosquito populations are constant,
2. humans and vectors are either susceptible or infectious at any given time and
3. humans are clear of human infection at a constant rate r once infected.

Infection can be acquired by a susceptible human from the bite of an infectious mosquito and the parasite can be acquired by a healthy mosquito by feeding on an infected human.

Adding Eqs 3.1-3.5, we will obtain an equation for the total human population with

$$\frac{dN}{dt} = B - \delta_H N. \tag{4.1}$$

Hence, throughout this section, we will consider $B = \delta_H N$ which preserves the human population constant. In endemic areas, longer infection recovery periods correspond to a higher transmission

intensity, in this case, the mosquito exposure. As the level of disease transmission increases, the recovery rate r tends to slow down. The transmission intensity (Λ) is represented as

$$\Lambda = a\frac{W}{N}, \tag{4.2}$$

whereby W represents the total number of infectious mosquitos, N is the total human population and a is the biting rate. The assumption made was that each infection lasted at a constant period of time which did not depend on any other infection occurring simultaneously. Thus, it can be shown that

$$r(\Lambda) = \frac{\Lambda}{e^{\frac{\Lambda}{r_0}} - 1}, \tag{4.3}$$

where $r(\Lambda)$ represents the effective recovery rate at a given transmission intensity (Λ). The initial recovery rate when the disease transmission is at the lowest is denoted as r_0, for instance when there is no infectious mosquitoes available.

Moreover, regular exposure to the parasite in return boosts an individual's immunity [16] leading to slower rates of loss of immunity. Using the same decaying transmission intensity, we obtained

$$\sigma(\Lambda) = \frac{\Lambda}{e^{\frac{\Lambda}{\sigma_0}} - 1}, \tag{4.4}$$

The transmission rate, also known as the force of infection, β is the per capita rate at which susceptible individuals gain the infection per unit time because of infectious bites. β depends on three factors which are :

1. human immune response which contributes to the probability reduction of developing malaria after receiving an infectious bite by a factor b,
2. number of infectious mosquitoes ,W per human hosts,
3. biting rate, a.

Thus, the force of infection, β can be expressed as

$$\begin{aligned} \beta &= b\frac{W}{N}a \\ &= b\Lambda. \end{aligned} \tag{4.5}$$

Here, both processes are controlled by the same biting rate, (a). However, the probability of per-bite transmission varies from vector to host (b) and host to vector (c). The constant per capita death rates act upon both the humans (δ_H) and mosquitoes (δ_M). Since populations are kept constant and can be divided in either susceptible classes or infectious classes, the state of the human-mosquito system can be expressed by only two variables; the fraction of the infectious humans (y) and the number of infectious mosquitoes per human (w). Hence, the temporal evolution of the state variables are as below

$$\frac{dw}{dt} = cay(m - w) - \delta_M w, \tag{4.6}$$
$$\frac{dy}{dt} = (baw + \beta_e)(1 - y) - (\delta_H + r)y, \tag{4.7}$$

where β_e is an external transmission rate (the rate at which susceptible humans gain the infection from outside the system) and m is the total mosquitoes per human.

The classical RM Model does not consider any external infection, thus $\beta_e = 0$ and absence of explicit human rate, $\delta_H = 0$ (which will be used as a small correction to the recovery rate, r). We can then divide the first equation by m and the system can be re-written as

$$\frac{dx}{dt} = cay(1 - x) - \delta_M x, \tag{4.8}$$
$$\frac{dy}{dt} = bamx(1 - y) - ry, \tag{4.9}$$

where x is the fraction of infectious mosquitoes. It is straightforward to calculate the stationary state by the intersection of the two analogous isoline

$$cay(1 - x) - \delta_M x = 0, \tag{4.10}$$
$$bamx(1 - y) - ry = 0. \tag{4.11}$$

The RM Model has two stationary equilibrium points, which are the disease-free equilibrium where $x = 0, y = 0$ and the endemic equilibrium (x=x∗,y=y∗) which is as follows

$$x* = \frac{a^2bcm - \delta_M r}{abm(ac + \delta_M)}, \tag{4.12}$$
$$y* = \frac{a^2bcm - \delta_M r}{ac(abm + r)}, \tag{4.13}$$

When superinfection is introduced as an effect of slowing down on the recovery rate r due to the transmission intensity [8], we will then show the coexisting stable stationary points for different parameter combinations. We will then observe the presence of a saddle node bifurcation as a model parameter crosses a certain threshold.

The Dietz function (Eq 4.14), acts as the influence of repeated infectious bites on the recovery rate, which here is expressed in terms of the dimensionless fraction of infectious mosquitoes, x. Thus, we obtain

$$r(x; a, m, r_0) = \frac{amx}{e^{\frac{amx}{r_0}} - 1}. \tag{4.14}$$

The effective recovery rate, r is no longer constant but slows down as the density of infectious mosquitoes per human increases for a given parameter set, as referred to Figure 4.1. As observed from the figure, as the biting rate a increases, the recovery rate decays faster.

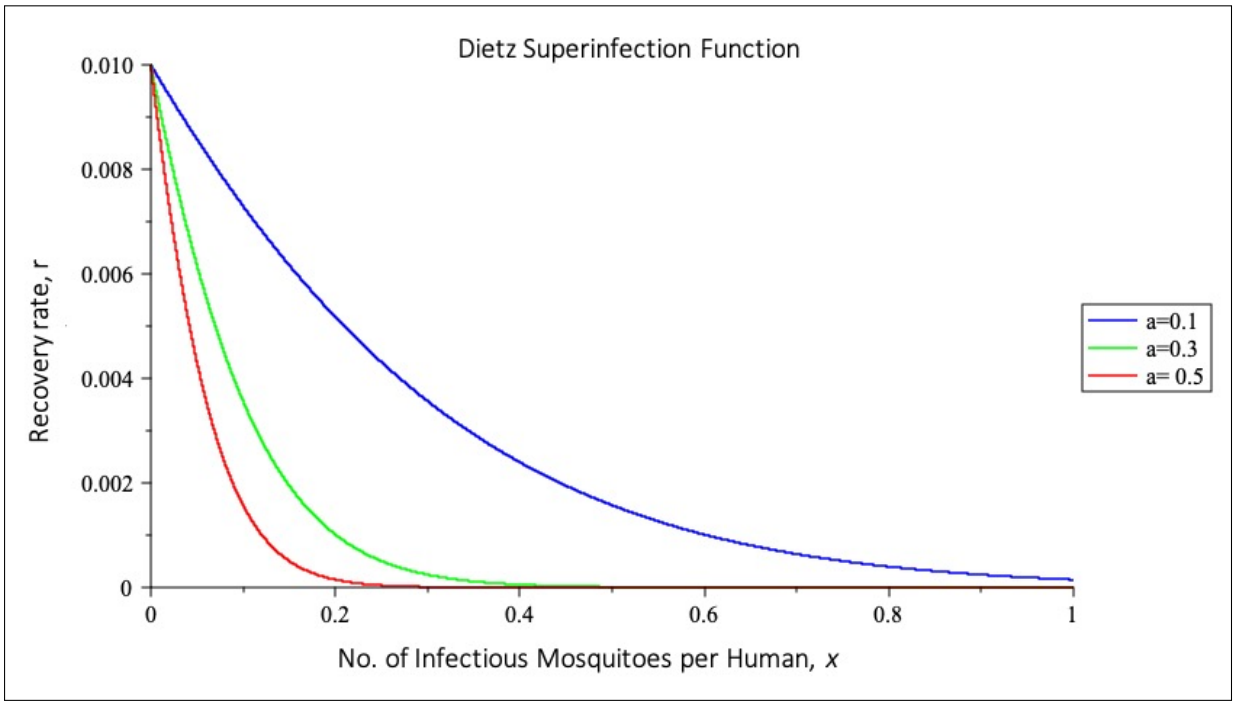

Figure 4.1: The diagram above shows the Dietz superinfection function for different values of biting rate, a. r represents the effective recovery rate whilst x represents fraction of infectious mosquitoes. The values of biting rate observed are $a = 0.1$, $a = 0.3$ and $a = 0.5$. The effective recovery rate declines as the number of infectious mosquitoes per human gets larger with sharper decay as the biting rate increases.

Bistability Conditions

To discover the conditions under which it is possible for multiple endemic states to exist, let us refer to the two isolines whose intersection defines the said states. Based on Eqn 4.11, the fraction of infectious humans can be written in terms of fraction of infectious mosquitoes

$$y = \frac{abmx}{abmx + r(x)}, \tag{4.15}$$

where $r(x)$ is the Dietz equation given by Eq (4.3). Let us call this function as $F_1(x)$. Using the same method on Eq 4.10, the fraction of mosquitoes can be expressed as

$$x = \frac{acy}{acy + \delta_M}, \tag{4.16}$$

which can be re-written as :

$$y = \frac{\delta_M x}{ac(1-x)}, \tag{4.17}$$

let us name this equation $F_2(x)$. This gives the fraction of infectious humans at the equilibrium for a given fraction of infectious mosquitoes. Thus, the two isolines can be shown by the functions $y = F_1(x)$ and $y = F_2(x)$.

We can find the intersection of $y = F_1(x)$ and $y = F_2(x)$ numerically. However, using this straightforward numerical method, it is difficult to obtain the analytic conditions of the model parameters which indicate the number of intersecting points. Hence, to approach this point analytically, let us analyse the curvature of the two isolines. Curvature analysis is crucial as they can describe the behaviour of the system.

For the 2nd isoline, $F_2(x)$ the first and second derivatives with respect to x are denoted as

$$F'_2(x) = \frac{\delta_M}{ac(1-x)^2}, \tag{4.18}$$

$$F''_2(x) = 2\frac{\delta_M}{ac(1-x)^3}, \tag{4.19}$$

In the range of $0 < x < 1$, both Eq 4.18 and Eq 4.19 are positive. Having them both positive means that the function $F_2(x)$ is an increasing function of x and its curvature will never change as the term that includes x is a fraction.

Next, let us analyse the 1st isoline, $F_1(x)$ and its first and second derivatives. First, let us consider the case where the recovery rate is a constant parameter, $r(x) = r_0$

$$F'_1(x) = \frac{abmr_0}{(abmx + r_0)^2}, \tag{4.20}$$

$$F''_1(x) = -2\frac{abmr_0}{(abmx + r_0)^3}. \tag{4.21}$$

Hence, since $x > 0$, the function $F_1(x)$ is also always increasing, since again, both Eq 4.20 and Eq 4.19 are positives. Thus, if the recovery is constant, $F_1(x)$ and $F_2(x)$ are both monotonically increasing but never change curvature with opposite curvatures which can be seen in Figure 4.2.

Only $F_1(x)$ can potentially demonstrate a curvature change as it is the only function dependent on the recovery rate, r. Let us analyse the second derivative of $F_1(x)$ when r is no longer constant but given by the Dietz equation (Eqn 4.3). Let us name the variable $e^{\frac{amx}{r_0}} \equiv A$ and we will obtain

$$F'_1(x) = \frac{b}{(b(A-1+1))^2}\frac{am}{r_0}A, \tag{4.22}$$

$$F''_1(x) = (\frac{am}{r_0})^2 Ab\frac{1-b-bA}{(1+b(A-1))^3}. \tag{4.23}$$

Here, the first derivative will always be positive, thus the isoline is a monotonic increasing function of x. The denominator of the second derivative will also always be positive. This means that the sign of the second derivative depends on the numerator

$$M(y) \equiv 1 - b - bA. \tag{4.24}$$

Therefore, we need to authenticate under which conditions this function will have different signs as these conditions are essential for the coexistence of non-trivial steady states.

By equating $M(y) = 0$ we can obtain the change of curvature, which is

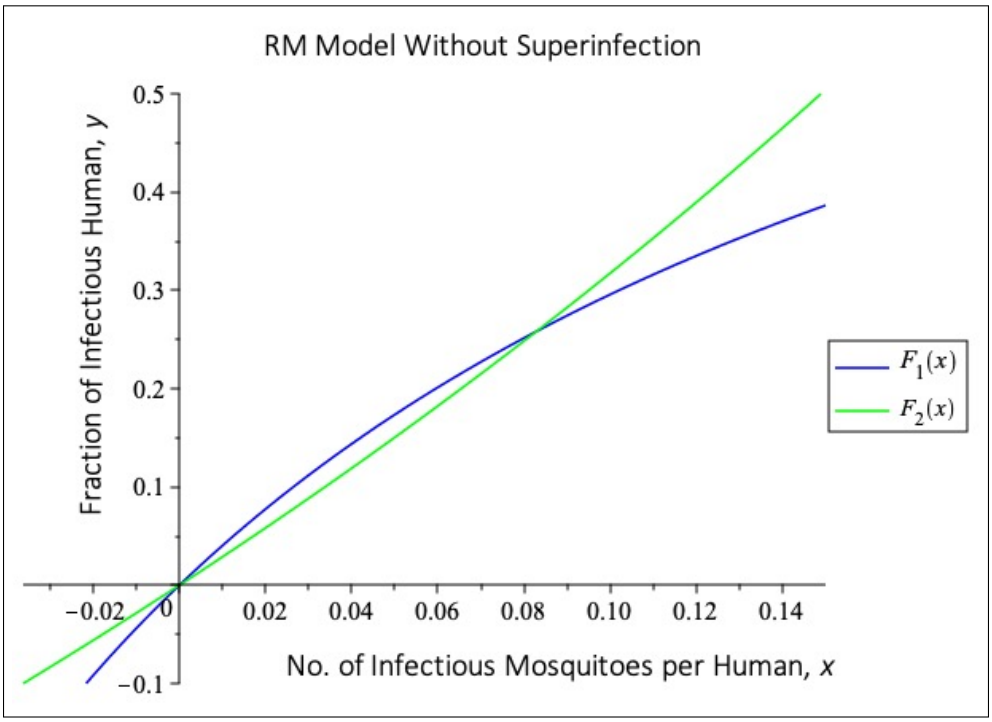

Figure 4.2: Diagram shows the isolines for $F_1(x)$ and $F_2(x)$ for a constant $r = 0.01$ with parameter $b = 0.2$. The graph shows an endemic stationary state, where the lines crosses at $x > 0, y > 0$.

$$x_i = \frac{r_0}{am} log(\frac{1-b}{b}), \tag{4.25}$$

and this equation is positive as long as $1 - b > b$, which requires $b < 0.5$. Hence, this will be our first condition. Then, we will obtain $F\,''_1(x) > 0 \quad \forall \quad x < x_i$ and $F\,''_1(x) < 0 \quad \forall \quad x > x_i$.

The change of curvature, x_i should occur at a value of less than 1 for it to be biologically meaningful. Particularly, it should be far less than its possible largest value. Hence, we will introduce a critical value, b_c and the condition will be true for when b is greater than b_c. The expression for the critical value, b_c is

$$b_c = \frac{1}{1 + e^{(\frac{am}{r_0}\frac{ac}{ac+\delta_M})}}. \tag{4.26}$$

In conclusion, by including superinfection to the two isolines system, we have proven that one of them is a monotonic increasing function with constant curvature and the other isoline is also a monotonic increasing function but changes sign at x_i (known as inflection point) for some parameters.

Thus, we are able to deduct the two important conditions for steady state to coexist. They can be interpreted in terms of the probability of infectivity, b as follows

$$b_c < b < 0.5, \tag{4.27}$$

and b_c is expressed as Eq 4.26 and is dependent on 5 other parameters. The critical value, b_c is bounded between 0 and 0.5 (based on Eq 4.25).

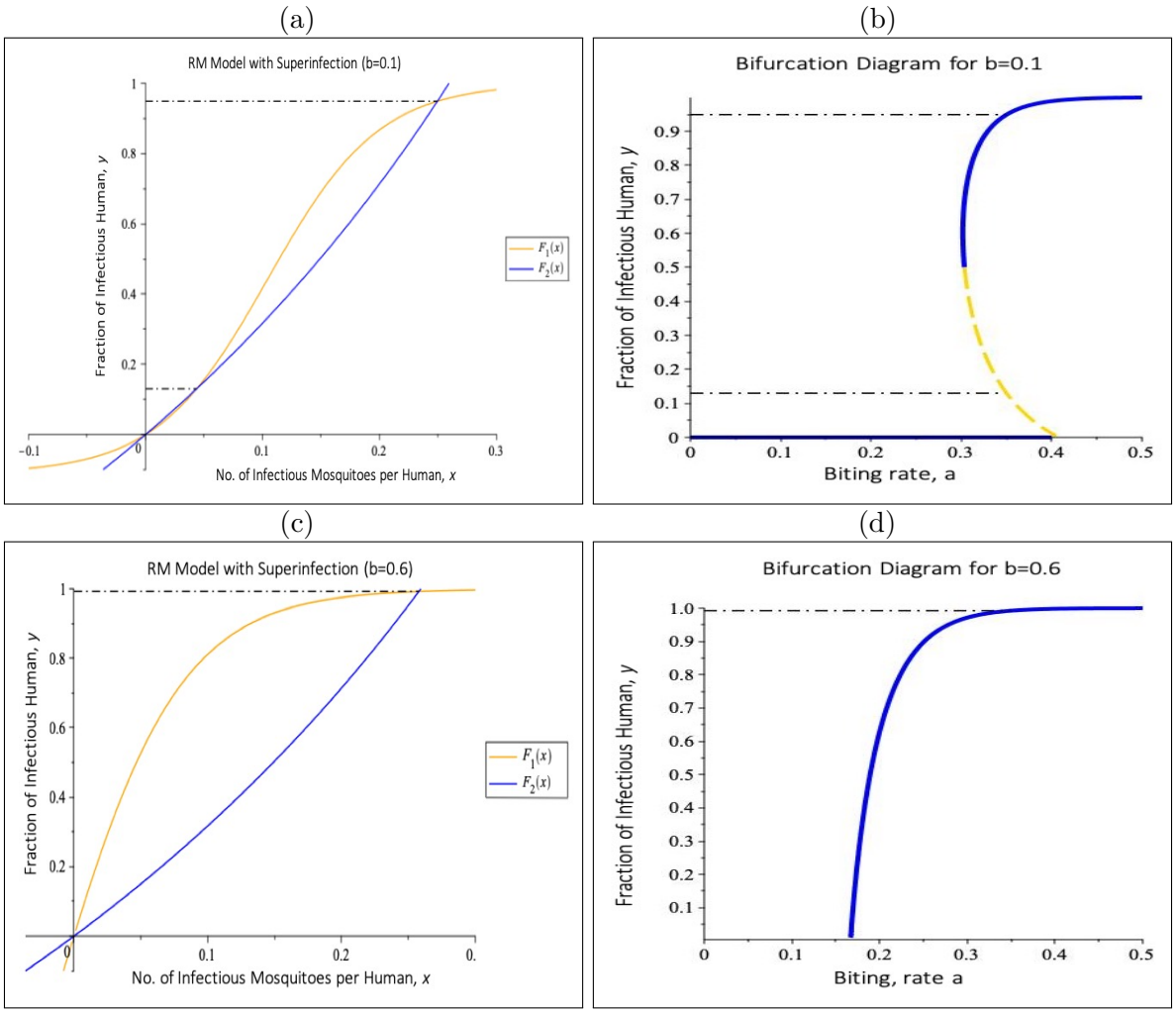

Figure 4.3: Diagram shows the inclusion of superinfection in Ross and MacDonald Model. On the top panels are for b=0.1. In (a) there is coexistence of endemic steady states in the phase plane fraction of infectious human, y against number of infectious mosquitoes per human, x. The bottom panels are for b=0.6. Even as the value of the biting rate varies, (c) there is always only one endemic equilibrium in the phase plane. The other parameters in these systems are kept constant. The right panels are the bifurcation diagrams. As observed in (b), there is a saddle-node bifurcation which is represented with unstable equilibrium states (dashed yellow lines) and stable equilibrium states (blue line). In (d) there is only stable equilibrium states (blue line).

In Figure 4.3, we can observe how the isolines intersection defines the steady states in the conventional which are represented on the left planes (Figure 4.3(a) and (c)). The superinfection affect is represented in these figures by comparing Figure 4.3(a) and (c) and Figure 4.3(b) and (d). The right figures are the bifurcation diagrams for the system for incremental biting rates, a. Whenever there is a bistability, a disease-free malaria equilibrium is located at the low equilibrium point(at $x = 0, y = 0$) because the classic RM Model does not include external force of infection. High malaria incidence occurs at high equilibrium point.

When the value of b is in the range of our condition ($0 < b < 0.5$) (refer Figure 4.3(a) and (c)), there is a saddle-node bifurcation. In this case, when the value of biting rate, a is at 0.35 the two curves cross at two points which correspond to both the stable and unstable endemic equilibria.

In conclusion, bistability shows that two different malaria incidence can occur within the same biting rate, with either low or high prevalence. Hence, this supports our hypothesis that spatial patterns can occur when there is bistability. This would explain why some areas would have higher malaria cases and some have lower, despite having the same biting rate occurring.

4.2 RM Model Spatial Pattern Analysis

Let us return to the RM classical model with added spatial derivatives, which are

$$\frac{dx}{dt} = cay(1-x) - \delta_M x + D_1 \nabla^2 x, \tag{4.28}$$

$$\frac{dy}{dt} = bamx(1-y) - ry + D_2 \nabla^2 y. \tag{4.29}$$

As shown in our result earlier, neither Figure 4.3(a) or Figure 4.3(b) are similar to Figure3.2(e) or (f). This would be an initial indicator that their Jacobian matrices about the steady state are not the same signs as both the cases discussed in Figure 3.2. Hence, intuitively this also indicates that there is no Turing instability in the RM model with and without superinfection (refer to Eq (4.28 and 4.29)) using the chosen parameters. Let us prove our intuition by plotting the graph for their respective eigenvalues $\lambda(k)$ and their wavenumber k which are shown in Figure (4.4) and (4.5, known as the dispersion curves.

Thus, as observed in Figure 4.4 and 4.5,the RM Model with given parameters shows no existence of Turing instability despite varying their diffusion rates, D. This is due to their Jacobian matrix evaluated at the steady states not having the properties needed for Turing instability to take place.

4.3 Reaction Diffusion Computation

The evolution of dynamical systems involving both time and space such as epidemic propagations and population dynamics can be described by Partial Differential Equations (PDEs). PDEs are commonly studied via numerical solutions as they are hard to be solved analytically. In this section, we will illustrate a reaction-diffusion simulation via PDE. Here, we simulate a system proposed by Alan Turing which displays mosquito spatial pattern in a set region. The simulations were computed in Python with spatial scale of 2×2 kilometers, which was based upon [28]. The code for the simulation is shown in Appendix A.3.

The Laplace operator function is defined by five-point stencil finite difference method based on [28], with domain $E = [-1, 1]^2$. The Laplacian operator is defined by

$$\nabla^2 x(z_1, z_2) \approx \frac{x(z_1 + h, z_2) + x(z_1 - h, z_2) + x(z_1, z_2 + h) + x(z_1, z_2 - h) - 4x(z_1, z_2)}{dz_1^2} \tag{4.30}$$

where z_1, z_2 are the spatial terms and h is sufficiently small. At each time step, the system was computed on the grid using discrete spatial derivatives (Eq 4.30). This method includes both time and space discretisation together with their derivatives replaced with their discrete equivalents. We take the Neumann boundary conditions, requiring the spatial derivatives of the variables with respect to the normal vectors to be zero on the domain's boundaries.

To ensure stability of unstable numerical methods, the Courant-Friedrichs-Lewy (CFL) condition has to be satisfied [25]. In order to meet this condition, the time step, dt must be sufficiently small and the values for diffusion has to be manipulated for the system to not blow up. The CFL condition is :

$$\frac{\chi \triangle t}{(\triangle x)^2} \leq \frac{1}{2} \tag{4.31}$$

where χ is the diffusion term, $\triangle t$ is the time step,dt and x is the domain.

The results obtained from this computation show the evolution of spatial patterns over time. Infectious mosquitoes are indicated in copper and if they do not appear it is represented in black on the figures.

Figure 4.6 (a) displays the values of infectious mosquitoes on the midpoint of the domain (a fixed point) over time. It shows that the system reaches equilibrium point $(x^*, y^*) \approx (0.85, 0.30)$

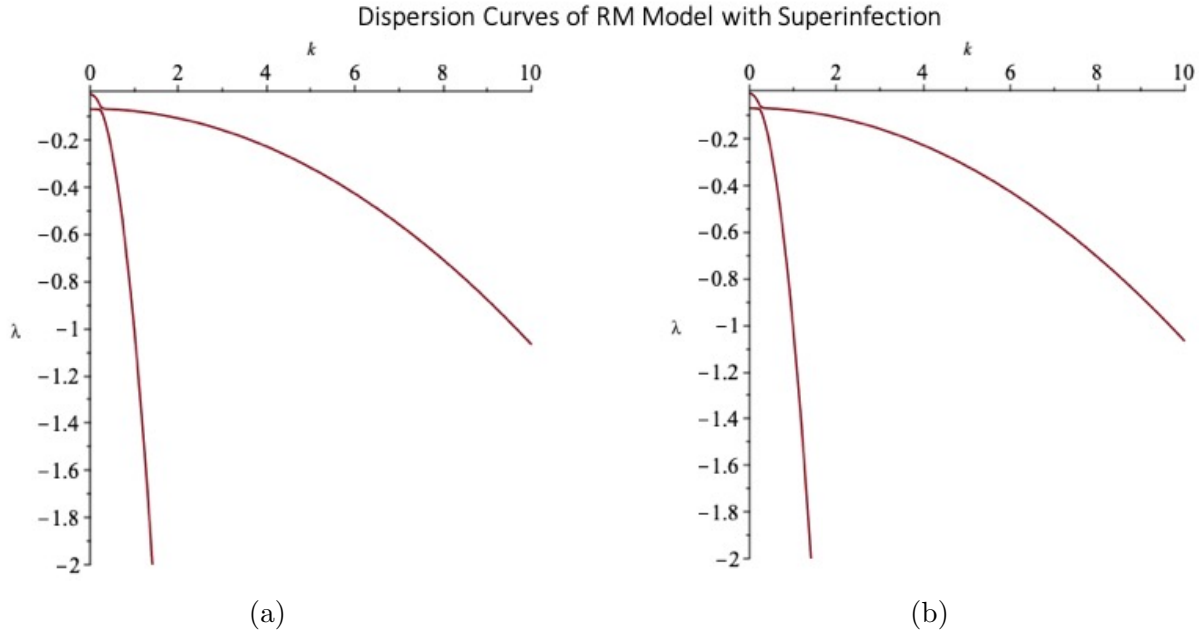

(a) (b)

Figure 4.4: The dispersion curves of RM Model with superinfection using Eqs 4.28 and 4.29 with parameters in Table A.2 in the Appendix. (a) is the system with value $D_1 = 1$ and $D_2 = 0.01$ and (b) is the value for $D_1 = 0.01$ and $D_2 = 1$. Despite changing the values of diffusion D, both the graphs look similar and does not portray any Turing instability with given parameters.

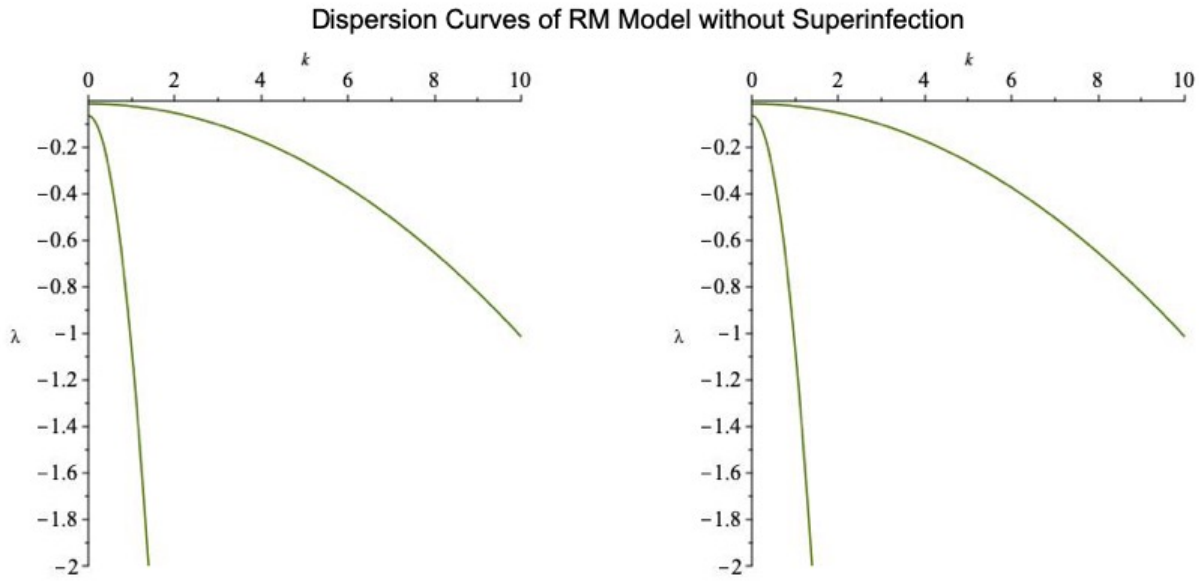

(a) (b)

Figure 4.5: The dispersion curves of RM Model without superinfection using Eqs 4.28 and 4.29 with parameters in Table A.2 in the Appendix. (a) is the system with value $D_1 = 1$ and $D_2 = 0.01$. (b)is the value for $D_1 = 0.01$ and $D_2 = 1$. Despite changing the values of diffusion D, both the graphs still look similar. Hence, we can conclude there is no Turing instability in the classic RM Model with given parameters.

when the diffusion is turned off ($D_1 = D_2 = 0$) and no spatial pattern can be observed as the results show only black figures. This supports Alan Turing's reasoning that spatial pattern do not occur when there is no diffusion.

We will now observe the behaviour of the spatial patterning using two sets of random initial conditions. At time step 2000, both the infectious humans and mosquitoes reach their equilibrium as shown in Figure 4.7 (a) and (c). Both the respective spatial patterns show that the system tends to a homogeneous pattern despite having random initial values. We expect the figure to reach a full homogeneous pattern with a longer time. Hence, our results show that without Turing instability, a system tends to a homogeneous spatial pattern. It is difficult, in our case, to manipulate time to be very large as the CFL condition will not be satisfied. This is also accompanied by a weak computer used for this research, which cannot handle big data memory storage well.

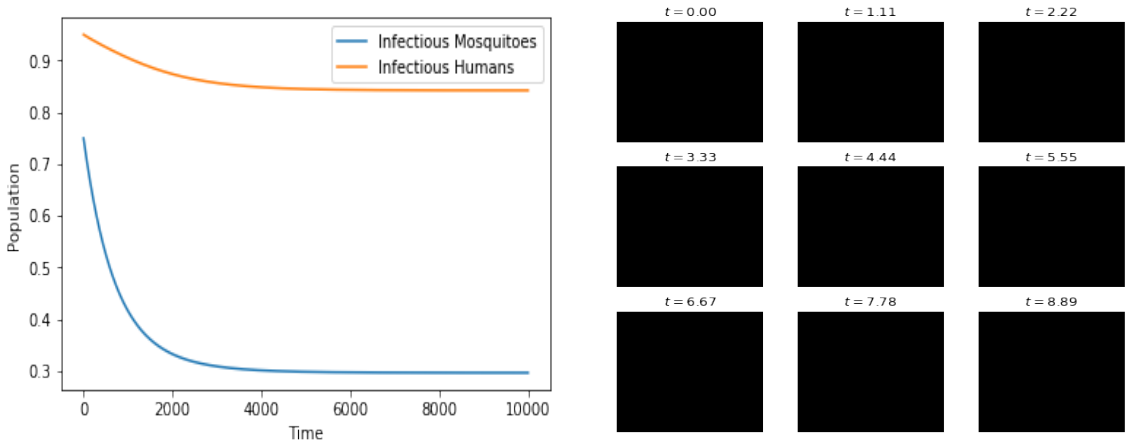

(a) (b)

Figure 4.6: Diagram shows the RM model reaction diffusion of Eqs 4.28 and 4.29 with parameters in Table A.2 when the diffusion is turned off.(a) shows the population dynamics of RM model and (b) displays the spatial pattern of RM model when diffusion is off.

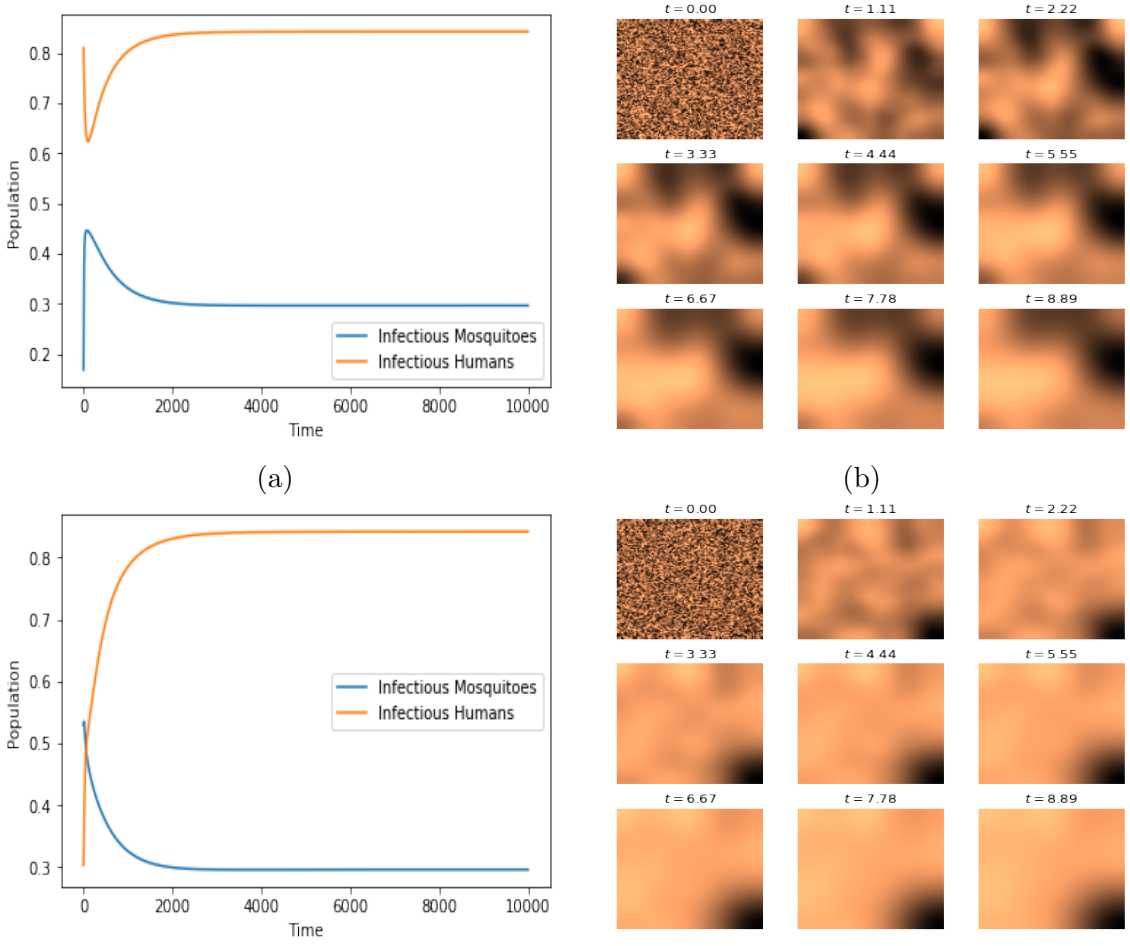

(a) (b)

(c) (d)

Figure 4.7: Computations with two sets of random initial conditions (a) and (c) with their respective spatial patterns (b) and (d). We used Eq 4.28 and 4.29 with parameters in Table A.2.(a) and (c) are the values of infectious mosquitoes at the midpoint of domain on every time step . The results show homogeneous pattern invading the whole domain in both (b) and (d).

Chapter 5

Extended Human-Mosquito Interaction Model

Now, we will focus on finding the existence of Turing instability in a system of 3 variables to observe the evolution of their spatial pattern. Since the dispersion curves are dependent on $\lambda(k)$, we need to find a system whereby the values of the eigenvalues are larger than zero to give rise to Turing instability.

With the knowledge of the dynamics of human-mosquito, we introduce a system with uninfected humans (H), infected humans (I), uninfected mosquitoes (M) and infected mosquitoes (P). The system of equations are as below

$$\frac{dH}{dt} = (b_H - d_H)H - I_{MH} + rI + D_1\nabla^2 H, \tag{5.1}$$
$$\frac{dI}{dt} = -d_H I + I_{MH} - rI + D_2\nabla^2 I, \tag{5.2}$$
$$\frac{dP}{dt} = -d_M P + I_{HM} + D_3\nabla^2 P, \tag{5.3}$$
$$\frac{dM}{dt} = (b_M - d_M)M - I_{HM} + D_4\nabla^2 M, \tag{5.4}$$

where $I_{MH} = cPH$ and $I_{HM} = bMI$ are the infection rates of humans and mosquitoes respectively. This system differs from the RM model such that human populations are not constant and human death rate, d_H is always smaller than human birth rate, b_H.

This human-mosquito system can be reduced to 3 equations as we assume that only the total numbers of uninfected mosquitoes (M) and infected mosquitoes (P) are constant. Hence, we have that $N = M + P$ where N is the total number of mosquitoes. The coefficients and other parameters from the above system is shown in Table 5.1. Thus, we can eliminate M using this assumption together with substituting the values of $I_{MH} = cPH$ and $I_{HM} = bMI$, we will obtain the new reduced system of equations as

$$\frac{dH}{dt} = (b_H - d_H)H - cPH + rI + D_1\nabla^2 H, \tag{5.5}$$
$$\frac{dI}{dt} = -d_H I + I_{MH} - rI + D_2\nabla^2 I, \tag{5.6}$$
$$\frac{dP}{dt} = -d_M P + b(N - P)I + D_3\nabla^2 P, \tag{5.7}$$

Model Parameter	Symbol	Value
Human birth rate	b_H	5.068e-5
Human death rate2	d_H	2.137e-5
Mosquito birth rate	b_M	0.636
Mosquito death rate	d_M	0.5
Total number of Mosquitoes	N	100
Recovery rate	r	0.01
Human Infection rate coefficient	c	0.5
Mosquito Infection rate coefficient	b	0.1

Table 5.1: Values of human-mosquito parameters.

and the values for diffusion rate, D for each class is set to be

$$D := \begin{pmatrix} D_1 & 0 & 0 \\ 0 & D_2 & 0 \\ 0 & 0 & D_3 \end{pmatrix} = \begin{pmatrix} 0.00001 & 0 & 0 \\ & 0.001 & 0 \\ 0 & 0 & 0.0001 \end{pmatrix}. \tag{5.8}$$

The steady states for this system is (H_0, I_0, P_0) which were found to be $(0.024, 0.033, 0.274)$. The Jacobian matrix, A for this system is

$$A := \begin{pmatrix} -cPH + b_H - d_H & 0 & -cH \\ cP & -d_H - r & cH \\ 0 & b(N-P) & -bI - d_M \end{pmatrix}_{(H_0, I_0, P_0)}. \tag{5.9}$$

Thus, to get the eigenvalues $\lambda(k)$ we need to find the solutions of $|\lambda I - A + Dk^2|$ where I is an identity matrix. The solutions obtained for $\lambda(k)$ are

$$\lambda^3 + 0.648\lambda^2 + 0.063\lambda + 0.00706 = 0. \tag{5.10}$$

The dispersion curve is obtained by plotting the solutions of Eq 5.10 which is shown in Figure 5.1. Next, we will observe the spatial patterning of the human mosquito model with two different diffusion rates (Eq 5.11 and Eq 5.8).

Therefore, based on our result, a homogeneous pattern takes place when there is no Turing instability in the system. The system reaches the homogeneous equilibrium in a short period of time as shown in Figure 5.2 and the pattern settles down. Even by running the computation with three different sets of initial conditions, the final spatial pattern for all the three cases converged to a homogeneous state, as shown in Figure 5.3.

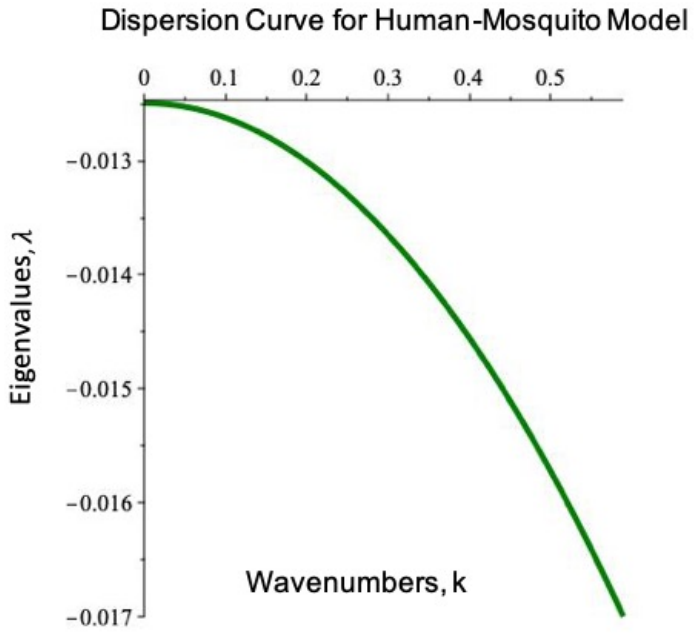

Figure 5.1: The dispersion curve of human-mosquito model using Eqs 5.5-5.7 with diffusion rates D in Eq 5.8 and parameters from Table 5.1. The system does not have Turing instability as the eigenvalues,$\lambda(k)$ are all negative.

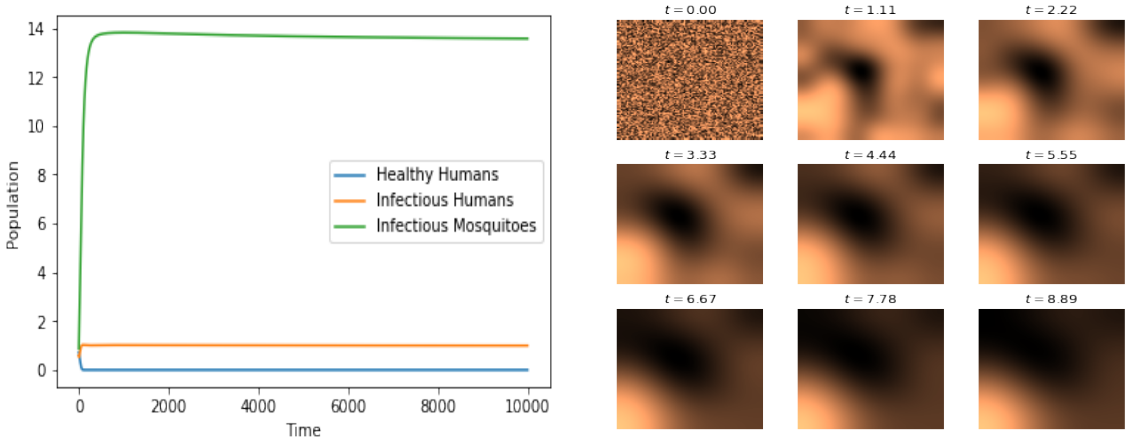

(a) (b)

Figure 5.2: Computations random initial conditions for Eqs 5.5-5.7 with diffusion rates D in Eq 5.8 and parameters from Table 5.1.(a) displays the values of infectious mosquitoes at the midpoint of domain on every time step . The results show homogeneous pattern invading the whole domain in (b) in the total time.

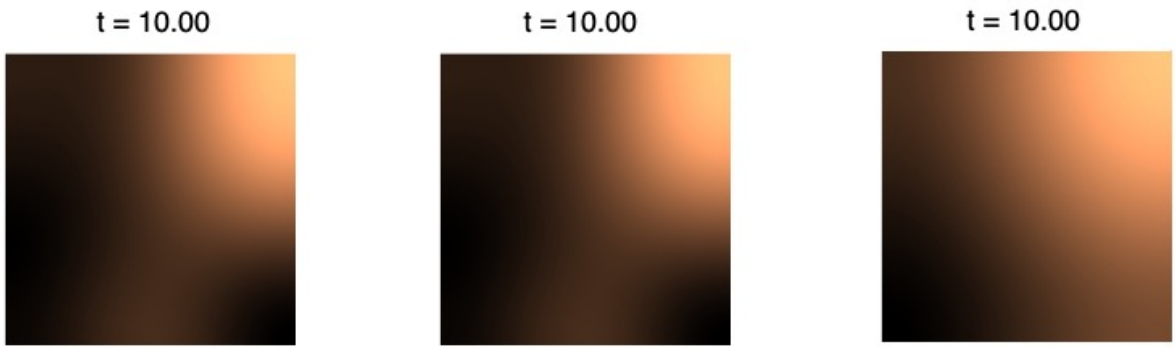

Figure 5.3: The final result for three sets of random initial conditions again for Eqs 5.5-5.7 with diffusion rates D in Eq 5.8 and parameters from Table 5.1. The results show homogeneous pattern invading the whole domain.

5.1 Turing Instability Existence

Next, let us observe what happens when we tune the values of the diffusion, D to

$$D := \begin{pmatrix} D_1 & 0 & 0 \\ 0 & D_2 & 0 \\ 0 & 0 & D_3 \end{pmatrix} = \begin{pmatrix} 0.001 & 0 & 0 \\ & 0.00001 & 0 \\ 0 & 0 & 0.0001 \end{pmatrix}. \tag{5.11}$$

These diffusion rates are chosen with the assumption that when humans are uninfected (H) they move and travel around more frequently with the help of vehicles, whilst infected humans(I) will move less as a portion of them will be in the hospital. Infected mosquitoes (P) will move at a rate slower than uninfected humans(H) because they only move to bite on humans but still at a higher rate than infected humans(I).

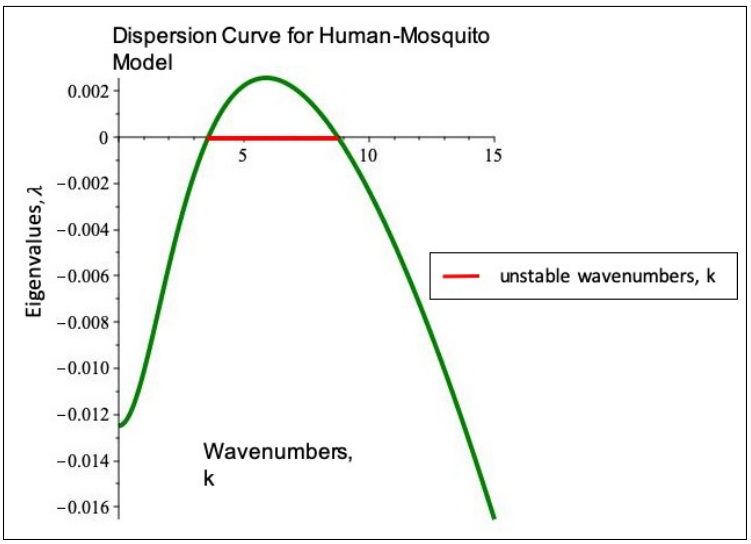

Figure 5.4: The dispersion curve of human-mosquito model using Eqs 5.5-5.7 with diffusion rates D in Eq 5.11 and parameters from Table 5.1. Turing instability occurs within the red line. This shows there is spatial pattern grow in this human-mosquito model.

The solutions of the eigenvalues $\lambda(k)$, again via $|\lambda I - A + Dk^2|$ are now

$$\lambda^3 + 0.648\lambda^2 + 0.0632\lambda + 0.00687 = 0. \tag{5.12}$$

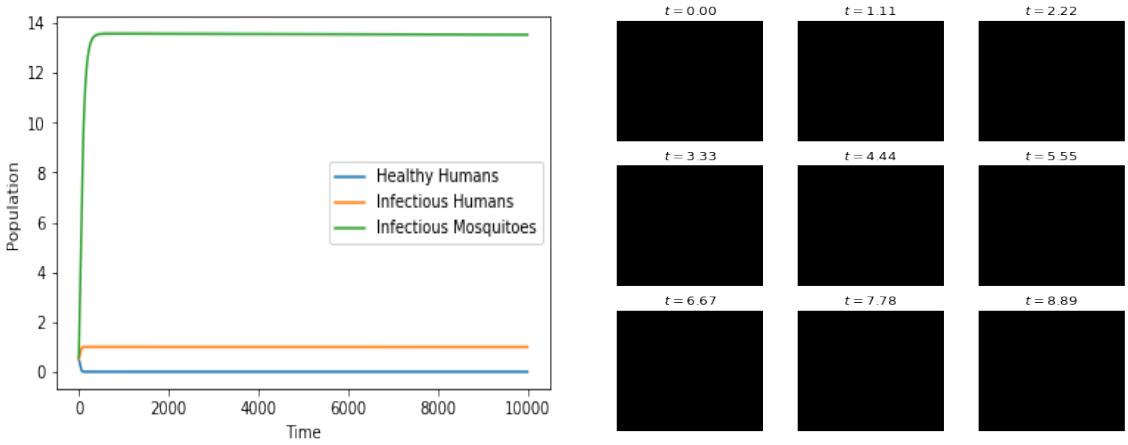

(a) (b)

Figure 5.5: The population dynamics when the diffusion are turned off for Eqs 5.5-5.7 and parameters from Table 5.1. The results show no spatial pattern when the diffusion is turned off.

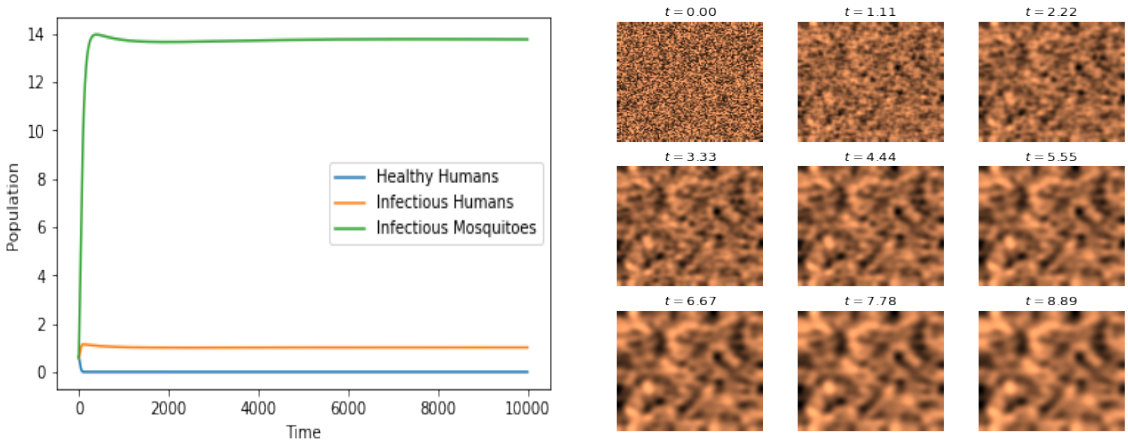

(a) (b)

Figure 5.6: The population dynamics for 5.5-5.7 with diffusion rates D in Eq 5.11 and parameters from Table 5.1 with random initial conditions.(a) displays the values of infectious mosquitoes at the midpoint of domain on every time step . The results in (b) show spatial pattern in the whole domain which never settles in the total time.

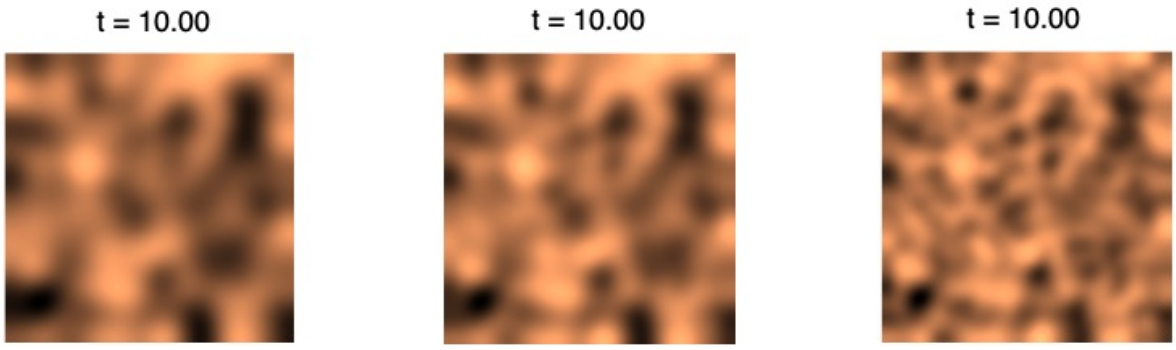

Figure 5.7: Figures show three different sets of initial conditions. On the final time there is still observable spatial patterning that never not settle down despite having different initial conditions. This computation is for Eqs 5.5-5.7 with diffusion rates D in Eq 5.11 and parameters from Table 5.1.

The dispersion curve for Eq 5.12 is shown in Figure 5.4. As there are positive eigenvalues, $\lambda(k)$, there is a Turing pattern in this system. This shows that diffusion rates determine the existence of a Turing pattern within a system. We now compute the evolution of the spatial pattern over time steps, t.

When the diffusion is turned off, no spatial pattern can be observed as shown in Figure 5.5. However, when we set the diffusion rate to those in Eq 5.11, we can observe spatial patterns evolving over time as shown in Figure 5.6. This pattern never becomes homogeneous because the system possesses Turing instability. More cases with three different sets of initial conditions were computed as shown in Figure 5.7, and again the spatial patterns do not converge to any homogeneous state. Hence, this result support our plausible hypothesis that spatial patterning includes Turing instability.

Chapter 6

Conclusion and Discussion

This thesis has supported plausible hypotheses that might cause patchiness emergence which include temperature variation, bistability and Turing pattern. Temperature variable affect the population of mosquitoes even by 1°C. The optimum temperature for mosquitoes to breed is in the range of 25°C to 28°C which explains as to why the number of mosquitoes in Uganda were the highest in years 2010 and 2016. It was also demonstrated that at high grounds and nature reserves, malaria does not exist. As we have investigated in Uganda, such areas never had any cases despite hospitable temperature. Thus, our findings show that geography also plays a role in malaria transmission.

Next, the Ross and MacDonald model(RM) shows bistability when a superinfection term is added with an existence of a saddle-node bifurcation. With the presence of superinfection, it produces a slowing-down effect on recovery rates as infectious bites gets higher [1]. Bistability only takes place in a certain parameter regions, which we have concluded that $b_c < b < 0.5$ where b is the probability of per-bite transmission varying from vector to host. Thus, the results conclude that superinfection introduces the probability of alternative steady states of low and high malaria prevalence with the same biting rate. This supports as a reasoning as to why some areas have higher malaria prevalence whilst other areas do not, giving rise to spatial pattern.

Our results show that without Turing instability, there are homogeneous spatial patterns. However, when a system posses Turing instability, there are inhomogeneous spatial patterns which never settle down. Thus, we conclude from our results that spatial patterns will never go homogeneous due to Turing instability. Hence, this supports one of our hypotheses that Turing instability might cause spatial patterns.

For future works, one should consider matching the parameters of the extended model to data and run the computation on a bigger domain with realistic values over a longer time. This study can be adopted for malaria control effort as in practice, even small changes in parameters would give rise to large changes in incidence, making malaria elimination more robust.

Bibliography

[1] D. Alonso, A. Dobson, and M. Pascual. Critical transitions in malaria transmission models are consistently generated by superinfection. *Philosophical transactions of the Royal Society of London. Series B, Biological sciences*, 374, 06 2019.

[2] N. Bacar. Mckendrick and kermack on epidemic modelling (1926-1927). In *A Short History of Mathematical Population Dynamics*, 01 2011.

[3] S. Baig and M. Sarfraz. Spatio-temporal analysis to predict environmental influence on malaria. *ISPRS - International Archives of the Photogrammetry, Remote Sensing and Spatial Information Sciences*, XLII-3:2615–2617, 05 2018.

[4] M. Baragatti, F. Fournet, M. Henry, S. Assi, H. Ouedraogo, C. Rogier, and G. Salem. Social and environmental malaria risk factors in urban areas of Ouagadougou, Burkina Faso. *Malaria journal*, 8:13, 02 2009.

[5] T. Bousema, J. Griffin, R. Sauerwein, D. Smith, T. Churcher, W. Takken, A. Ghani, C. Drakeley, and R. Gosling. Hitting hotspots: Spatial targeting of malaria for control and elimination. *PLoS medicine*, 9, 01 2012.

[6] F Cox. History of the discovery of the malaria parasites and their vectors. *Parasites and vectors*, 3:5, 02 2010.

[7] S. David, C. Drakeley, C. Chiyaka, and S. Hay. A quantitative analysis of transmission efficiency versus intensity for malaria. *Nature communications*, 1:108, 11 2010.

[8] K. Dietz, L. Molineaux, and A. Thomas. A malaria model tested in the African Savannah. *Bulletin of the World Health Organization*, 50:347–57, 02 1974.

[9] P. Gething, P. Patil, L. Smith, A. Guerra, R. Elyazar, L. Johnston, J. Tatem, and S. Hay. A new world malaria map: Plasmodium falciparum endemicity in 2010. *Malaria Journal*, 10(1):378, 12 2011.

[10] B. Grenfell and A. Dobson. *Ecology of Infectious Diseases in Natural Populations*. Publications of the Newton Institute. Cambridge University Press, 1995.

[11] S. Hay, C. Guerra, A. Tatem, A. Noor, and R. Snow. The global distribution and population at risk of malaria: Past, present, and future. *The Lancet infectious diseases*, 4:327–36, 06 2004.

[12] C. Hayes, A. Wheelock, J. Normark, M. Wahlgren, S. Goto, and C. Wheelock. Enlistment of omics technologies in the fight against malaria: Panacea or pandora's box? *Journal of Pesticide Science - J PESTIC SCI*, 31:263–272, 01 2006.

[13] E. Hempelmann. *History of Malaria*. 07 2010.

[14] A. Jain. Malaria, mosquitoes and the legacy of ronald ross - a commentary. *Annals of Community Health*, 1:8–12, 12 2013.

[15] J. Landier, S. Rebaudet, R. Piarroux, and J. Gaudart. Spatiotemporal analysis of malaria for new sustainable control strategies. *BMC Medicine*, 16(1):226, Dec 2018.

[16] J. Lavine, A. King, V. Andreasen, and O. Bjrnstad. Immune boosting explains regime-shifts in prevaccine-era pertussis dynamics. *PLOS ONE*, 8(8):1–8, 08 2013.

[17] P. Macharia, E. Giorgi, A. Noor, E. Waqo, R. Kiptui, E. Okiro, and R. Snow. Spatio-temporal analysis of plasmodium falciparum prevalence to understand the past and chart the future of malaria control in kenya. *Malaria Journal*, 17(1):340, 9 2018.

[18] R. Miranda Franco and A. Casta Vlez. [Eradication of malaria in Puerto Rico]. *Revista panamericana de salud pblica = Pan American journal of public health*, 2:146–50, 09 1997.

[19] E. Mordecai, K. Paaijmans, L. Johnson, C. Balzer, T. Ben-Horin, E. Moor, A. McNally, S. Pawar, S. Ryan, T. Smith, and K. Lafferty. Optimal temperature for malaria transmission is dramatically lower than previously predicted. *Ecology letters*, 16 1:22–30, 2013.

[20] P. Müller, M. Donnelly, and H. Ranson. Transcription profiling of a recently colonised pyrethroid resistant anopheles gambiae strain from ghana. *BMC genomics*, 8:36, 02 2007.

[21] J. Murray. *Mathematical Biology II: Spatial Models and Biomedical Applications*, volume 18 of *Interdisciplinary Applied Mathematics*. Springer New York, 2003.

[22] The University of Oxford. Malaria atlas project. http://map.ox.ac.uk/. Accessed: 2019-08-29.

[23] World Health Organization. Malaria. http://www.who.int/news-room/fact-sheets/detail/malaria.

[24] MACEPA Path. Making malaria history. http://www.makingmalariahistory.org/. Accessed: 2019-08-29.

[25] D Peterseim and M Schedensack. Relaxing the cfl condition for the wave equation on adaptive meshes. *Journal of Scientific Computing*, 72, 02 2017.

[26] Climate Change Knowledge Portal. Historical data. http://datacatalog.worldbank.org/dataset/climate-change-knowledge-portal-historical-data.

[27] R. Ross. *The Prevention of Malaria*. Dutton, 1910.

[28] C. Rossant. *IPython Interactive Computing and Visualization Cookbook*. Packt Publishing, 2014.

[29] E. Samba. The burden of malaria in Africa. *Africa health*, 19:17, 02 1997.

[30] David L. Smith, Katherine E. Battle, Simon I. Hay, Christopher M. Barker, Thomas W. Scott, and F. Ellis McKenzie. Ross, macdonald, and a theory for the dynamics and control of mosquito-transmitted pathogens. *PLOS Pathogens*, 8(4):1–13, 04 2012.

[31] D.L Smith, J. Dushoff, and F.E McKenzie. The risk of a mosquito-borne infection in a heterogeneous environment. *PLoS Biology*, 2:113 – 116, 2004.

[32] L. Torres-Sorando and D. Rodrguez. Models of spatio-temporal dynamics in malaria. *Ecological Modelling*, 104, 12 1997.

[33] World Health Organization. Unicef. Achieving the malaria MDG target: reversing the incidence of malaria 2000-2015. http://www.who.int/malaria/publications/atoz/9789241509442/en. Sep 2015.

[34] D. Weiss, T. Lucas, M. Nguyen, A. Nandi, D. Bisanzio, K. Battle, E. Cameron, K. Twohig, D. Pfeffer, J. Rozier, H. Gibson, P. Rao, D. Casey, A. Bertozzi-Villa, E. Collins, U. Dalrymple, N. Gray, J. Harris, R. Howes, and P. Gething. Mapping the global prevalence, incidence, and mortality of plasmodium falciparum, 2000-17: a spatial and temporal modelling study. *The Lancet*, 393, 06 2019.

[35] J. Zulueta. Malaria and ecosystems: from prehistory to posteradication. *Parassitologia*, 36 1-2:7–15, 1994.

Appendix A

A.1 Human-Mosquito Submodels Parameters

Model Parameter	Symbol	Value
Human parameters		
Immunity loss rate	σ_0	0.00067
Recovery rate ($I \rightarrow R$)	r_0	0.0063
Exposed number	n_H	1
Incubation rate	γ_H	0.05
External force of infection	β_e	1e-0.5
Detection probability	χ	0.2
Recovery rate ($C \rightarrow S$)	ρ	0.2
Case probability	η	0.01
Incubation rate	γ_H	0.05
External force of infection	β_e	1e-0.5
Detection probability	χ	0.2
Recovery rate ($C \rightarrow S$)	ρ	0.2
Case probability	η	0.01
Recovery rate ($C \rightarrow I$)	ν	0.1
Adult mosquito parameters		
Biting rate	a	0.3
Per bite vector to host infectivity probability ($M \rightarrow H$)	b	0.5
Per bite host to vector infectivity probability ($H \rightarrow M$)	c	0.2
Death rate	δ_M	0.04
Larva parameters		
No. of larval recruits per oviposition event	N_L	66
Carrying capacity	K_0	3e04
Development rate	d_L	0.067
Death rate	δ_L	0.5
Plasmodium related parameters		
Exposed number	n_P	1
Incubation rate	γ_P	0.05

Table A.1: Parameter values for the human and mosquito submodels.

A.2 Ross-MacDonald Model Parameters

Model Parameter	Symbol	Value
Mosquito parameters		
Biting rate	a	0.35
Infectivity probability ($H \to M$)	c	0.05
Mosquito mortality rate	δ_M	0.05
No. of mosquitoes per human	m	0.6
Human parameters		
Infectivity probability ($M \to H$)	b	0.1
External transmission rate	β_e	0
Human mortality rate	δ_H	0
Recovery rate ($I \to S$)	r_0	0.01

Table A.2: Parameter values for Ross and MacDonald Model

A.3 Code for Spatial Pattern

```
import numpy as np
import matplotlib.pyplot as plt
import random
%matplotlib inline

Tscale=20 # to scale time
b_H = 0.00005068*Tscale
d_H = 0.00002137*Tscale
d_M = 0.636*Tscale
N = 100
r = 0.01*Tscale
c = 0.5*Tscale
b = 0.1*Tscale
D1 = 0.00001*Tscale #diffusion values, can be tuned to fit data
D2 = 0.001*Tscale
D3 = 0.0001*Tscale

size = 100  # size of the 2D grid
dx = 2. / size  # space step
T = 10  # total time
dt = .001  # time step
n = int(T / dt)  # number of iterations

H = np.random.rand(size, size) #uninfected humans
I = np.random.rand(size, size) #infected humans
P = np.random.rand(size, size) #infected mosquitoes

def laplacian(Z): # Laplacian function using forward difference method
    Ztop = Z[0:-2, 1:-1]
    Zleft = Z[1:-1, 0:-2]
    Zbottom = Z[2:, 1:-1]
```

```
    Zright = Z[1:-1, 2:]
    Zcenter = Z[1:-1, 1:-1]
    return (Ztop + Zleft + Zbottom + Zright -
            4 * Zcenter) / dx**2

def show_patterns(P, ax=None): # show spatial pattern,
    ax.imshow(P, cmap=plt.cm.copper,    # copper shows infectious mosquitoes
              interpolation='bilinear',
              extent=[-1, 1, -1, 1])
    ax.set_axis_off()

fig, axes = plt.subplots(3, 3, figsize=(8, 8))
step_plot = n // 9
# We simulate the PDE with the finite difference
# method.


H_value=[]
I_value=[]
P_value=[]


for i in range(n):
    # We compute the Laplacian of H,I and P.
    deltaH = laplacian(H)
    deltaI = laplacian(I)
    deltaP = laplacian(P)

    # We take the values of H,I and P inside the grid.
    Hc = H[1:-1, 1:-1]
    Ic = I[1:-1, 1:-1]
    Pc = P[1:-1, 1:-1]
    # We update the variables.
    H[1:-1, 1:-1], I[1:-1, 1:-1], P[1:-1, 1:-1] = \
        Hc + dt * ((b_H - d_H) * Hc - c * Pc * Hc + r * Ic + D1 * deltaH) ,\
        Ic + dt * (-d_H * Ic + c * Pc * Hc - r * Ic + D2 * deltaI),\
        Pc + dt * (-d_M * Pc + b * (N-Pc) * Ic + D3 * deltaP)
    # Neumann conditions: derivatives at the edges
    # are null.
    for Z in (H, I, P):
        Z[0, :] = Z[1, :]
        Z[-1, :] = Z[-2, :]
        Z[:, 0] = Z[:, 1]
        Z[:, -1] = Z[:, -2]

    # values of H,I snd P at midpoint of domain
    if  i < T* step_plot  :
        H_value.append(H[49][49])
        I_value.append(I[49][49])
        P_value.append(P[49][49])
```

```
    # We plot the state of the system at
    # 9 different times.
    if i % step_plot == 0 and i < 9 * step_plot:
        ax = axes.flat[i // step_plot]
        show_patterns(P, ax=ax)
        ax.set_title(f'$t={i␣*␣dt:.2f}$')


plt.figure()
plt.plot(H_value,label="Healthy␣Humans")
plt.plot(I_value,label="Infectious␣Humans")
plt.plot(P_value,label="Infectious␣Mosquitoes")
plt.xlabel("Time")
plt.ylabel("Population")
plt.legend();
plt.show()
```

Listing A.1: This is the code used to run the simulation for spatial pattern.